ACS APPLIED ENERGY MATERIALS
Cite This: ACS Appl. Energy Mater. 2018, 1, 4824−4839
Article
www.acsaem.org

Ammonia Synthesis by Radio Frequency Plasma Catalysis: Revealing the Underlying Mechanisms

Javishk Shah,[†] Weizong Wang,[‡] Annemie Bogaerts,*[,‡] and Maria L. Carreon*[,†]

[†]Russell School of Chemical Engineering, The University of Tulsa, Tulsa, Oklahoma 74104, United States
[‡]Department of Chemistry, Research Group PLASMANT, University of Antwerp, Universiteitsplein 1, 2610 Antwerp, Belgium

Supporting Information

ABSTRACT: Nonthermal plasma is a promising alternative for ammonia synthesis at gentle conditions. Metal meshes of Fe, Cu, Pd, Ag, and Au were employed as catalysts in radio frequency plasma for ammonia synthesis. The energy yield for all these transition metal catalysts ranged between 0.12 and 0.19 g-NH_3/kWh at 300 W and, thus, needs further improvement. In addition, a semimetal, pure gallium, was used for the first time as catalyst for ammonia synthesis, with energy yield of 0.22 g-NH_3/kWh and with a maximum yield of ∼10% at 150 W. The emission spectra, as well as computer simulations, revealed hydrogen recombination as a primary governing parameter, which depends on the concentration or flux of H atoms in the plasma and on the catalyst surface. The simulations helped to elucidate the underlying mechanism, implicating the dominance of surface reactions and surface adsorbed species. The rate limiting step appears to be NH_2 formation on the surface of the reactor wall and on the catalyst surface, which is different from classical catalysis.

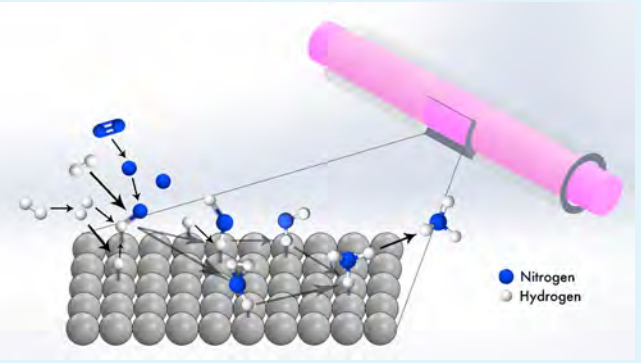

KEYWORDS: *plasma catalysis, ammonia synthesis, radio frequency plasma, molten metal, transition metal meshes*

INTRODUCTION

Ammonia production is one of those processes that eagerly call for alternative synthesis strategies. With ammonia currently synthesized through thermal catalysis at high temperature and pressure, alternatives such as synthesis by plasma technology, which can be sustained through solar/wind-produced electricity, are of great interest. However, a major roadblock to design an effective plasma-assisted process for ammonia production is the lack of fundamental information about this process, especially when using radio frequency (RF) plasma.

Ammonia is currently produced via the Haber−Bosch process, which is typically performed at 450−600 °C and 150−350 bar in the presence of a catalyst,[1−6] making it the most energy-intensive process in the chemical industry. With global ammonia production at ∼141 million tons per year in 2015[1] and projected to ∼249.4 million tons per year in 2018, the Haber-Bosch process consumes 1−2% of the world's energy, uses 2−3% of the world's natural gas output, and emits over 300 million metric tons of CO_2 each year.[7−9] These numbers partly arise from the need to separate nitrogen from air via cryogenic distillation and to source hydrogen from (typically) natural gas,[10] but a significant part of the energy consumption is because of the nature of the reaction itself.

The overall reaction for ammonia production is $3H_2 + N_2 \leftrightarrows 2NH_3$ $\Delta H_{298} = -10.97$ kcal/mol. The reaction enthalpy indicates that the reaction is thermodynamically favored at low temperature. However, the critical elementary step of N_2 dissociation presents a large free energy of activation, even on widely used heterogeneous catalysts. High temperature is needed to overcome the barrier, but this forces the use of high pressure to make the equilibrium favor the reaction again via Le Chatelier principle. It is clear that the kinetic stability of the N_2 triple bond ultimately makes the "fixation" of nitrogen an energy intensive process.[11−13] It is difficult to dissociate the triple bond of nitrogen because the molecule does not readily accept[14] or donate electrons.[15,16] The strengths of the N_2 triple, double and single bonds are 225, 100, and 39 kcal/mol, respectively.[11,17] Hence, even the current best catalysts still need to operate at temperatures of 500−600 °C or higher to achieve practical dissociation rates.[11] It is widely accepted that thermally catalyzed ammonia synthesis follows the Langmuir−Hinshelwood (LH) mechanism[18] (see Table S1).

Ammonia is used to produce plastics, synthetic fibers and resins, explosives, and numerous chemical compounds, but the major driving force behind ammonia synthesis is its use in fertilizers, including its direct application as anhydrous ammonia. Indeed, urea, ammonium nitrates, and ammonium phosphates are among the most important ammonia-derived chemicals. Given its impact on crop yield, the cost of ammonia has a direct impact on the pricing of food. Besides its impact in

Received: June 4, 2018
Accepted: August 29, 2018
Published: August 29, 2018

DOI: 10.1021/acsaem.8b00898
ACS Appl. Energy Mater. 2018, 1, 4824−4839

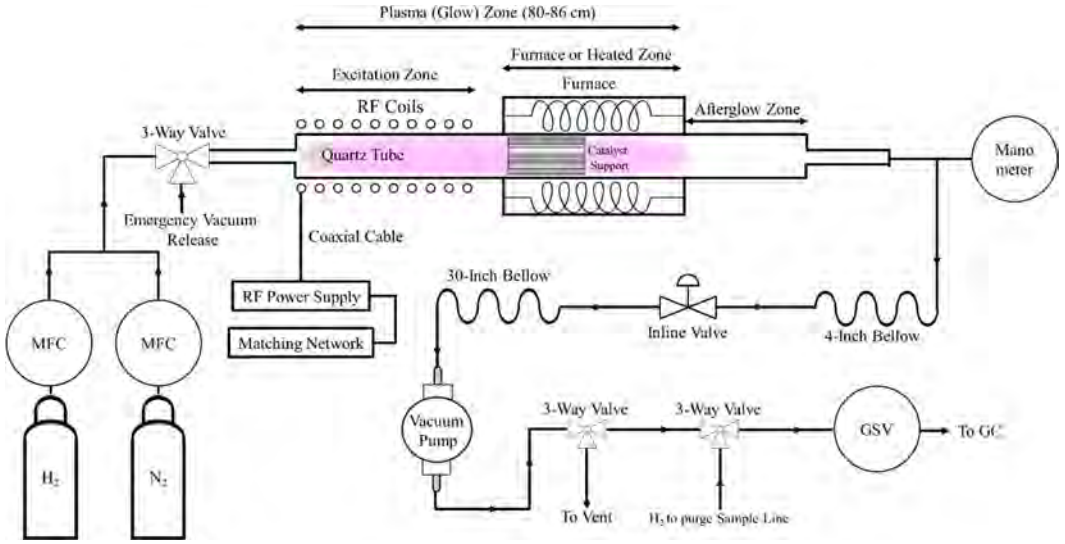

Figure 1. Schematic of the in-house built RF plasma reactor and surrounding equipment for gas inlet and outlet.

the food industry,[19] ammonia could have an impact in the transportation sector,[20−23] by potentially providing a long-term, zero-carbon emission fuel with a projected two-century lifespan.[24,25] Additionally, since one mole of ammonia contains 1.5 mol of hydrogen, 17.8 wt % of hydrogen or 108 g_{H_2}/L, are "stored" in liquid ammonia at 20 °C, which vastly surpasses the storage capacity (25 g/L) of traditionally studied hydrogen storage materials, such as metal hydrides.[26] Thus, by leveraging established methods and facilities for ammonia storage and handling, it could be feasible to implement an "ammonia economy,"[27] especially considering that ammonia could be synthesized from renewable feedstock, for example, hydrogen from biomass.[28,29]

The production of ammonia from renewable feedstock could also spur small plants at remote locations that could produce ammonia for use of local farmers. It is important to note, however, that the Haber−Bosch process is only economically feasible at large scale. Hence, alternative technologies need to be explored for the case of small scale synthesis of ammonia, especially if the processes could be powered through "renewable" electricity and performed at milder conditions. This prospect could be accomplished via plasma-based ammonia synthesis.

Plasma-based ammonia synthesis has been investigated to accelerate the rupture of the triple nitrogen bond at low temperature using different plasma discharges. A detailed overview of the state of the art is given in the Supporting Information (Table S2). Notably, nonthermal atmospheric plasma was able to synthesize ammonia successfully with enough yield for practical application (0.2−3.5%)[30−38] and with some exceptions even up to 7 and 9[39]%,[40,41] although the yield was highly dependent on the flow rate of N_2 to the reactor.[30−38] The use of catalyst-loaded ceramic membranes to achieve yields of 2%[30] is highly notable, but the membrane decreases the flow velocity of reactants, resulting in slow production rates. Most recently, nonthermal atmospheric plasma with metallic copper wool as catalyst led to an ammonia yield of 3.5% at room temperature.[38] Finally, Ru-promoted catalyst was reported to increase the yield to 7% in a DBD reactor,[40] and Ni supported on $BaTiO_3$ beads as catalyst resulted in the highest yield of 9% reported in a DBD plasma.[41]

Previous reports[38] demonstrated that meshes are one of the most effective catalyst configurations in DBD reactor. For comparison purposes when using a copper rod, the ammonia yields that we observed were lower as compared to wool like copper. Specifically, the yield was 0.83% for rod versus 2.6% for wool like copper. Furthermore, the commercial availability of these pellets is limited, and when available they are more expensive than the meshes.

Most studies on plasma-based ammonia synthesis are based on atmospheric pressure dielectric barrier discharge plasmas. Very few reports exist on the synthesis of ammonia from nitrogen−hydrogen using low pressure (0.01−10 Torr) RF discharges.[34,42−45] Despite the need of using a pump to generate vacuum, RF plasma sources are by far the most common employed in the semiconductor industry.[46] This offers the advantage of employing a source widely accepted and adapted to the industrial scale, plus the knowledge that this conveys, that is, operation and repair. In previous RF plasma-assisted ammonia reports, molecular sieves, such as 13X, were used for ammonia adsorption and the amount adsorbed was determined by the Kjeldahl method.[45] The maximum ammonia yield reported when using only plasma (no catalyst) was found to be ∼0.5 mmol/g-zeolite 13X. Typical reaction conditions were 650 Pa (∼5 Torr), 20 sccm (1.2 dm^3/h), 3 h at 130 W-180 W using a nitrogen−hydrogen mixture of 4:1.[34,42−45] The effect of Fe wire and its loading pattern as catalyst were studied, but the reaction stabilization point was never reached even after 3 h, leaving a lot of unanswered questions about the reaction scheme.[45] Furthermore, the combined effect of the plasma power and different catalysts on the ammonia yield has not been explored yet. Also, to our knowledge, there is no clear proposed mechanism for the synthesis of ammonia under RF plasma exposure. Evidence from the above-mentioned reports indicates that a lot of new insight is needed about the reaction kinetics and mechanism of the process, especially when using RF plasma.

In the present Article, we demonstrate unprecedented yields, as high as ∼19% when employing Au mesh and ∼10% when employing molten Ga as catalysts at suitable conditions.

In addition, we provide fundamental information about the nature of the reactive processes occurring during RF plasma-assisted ammonia synthesis, as a function of plasma power and

DOI: 10.1021/acsaem.8b00898
ACS Appl. Energy Mater. 2018, 1, 4824−4839

Table 1. Overview of the Species Included in the Model

molecules in ground state and in various electronically excited levels[a]	atoms	surface-adsorbed species	charged species
H_2, H_2 ,NH, NH_2, NH_3, N_2(A3), N_2(B3), N_2(C3), N_2(a′1), H_2(B1), H_2(B3), H_2(C3), H_2(A3)	H, N	H(s), N(s), NH(s), NH_2(s)	H_2^+, N_2^+, H^+, N^+, NH^+, NH_2^+, NH_3^+, NH_4^+, H_3^+, N_2H^+, e^-

[a]The notations of these electronically excited levels are taken from ref 51.

plasma-catalyst combination. Furthermore, through the integration of simulations and experiments, and using a unique experimental set up designed specifically for this task, we provide a close view of this nonthermal plasma approach.

EXPERIMENTAL SECTION

The experiments were performed in an *in-house built* plasma reactor (Figure 1). The reaction was conducted by introducing nitrogen (Praxair, 99%) and hydrogen (Praxair, 99.99%) at a 1:4 N_2:H_2 ratio to the reaction chamber using mass flow controllers. This ratio has also been reported in literature as the optimum ratio for plasma-based ammonia synthesis.[30,34,36,47] The nitrogen and hydrogen flow rates were 4 and 16 sccm, respectively. The plasma was ignited using an RF Power Supply with a Matching Network from Seren IPS, Inc. The typical reaction pressure and temperature were 0.26 Torr and 400 °C, respectively. The gas temperature is assumed to be 400 °C, controlled by the furnace temperature as the plasma itself will not give much heating at this low pressure. The plasma excitation was started when the furnace reached the desired temperature. Metal mesh catalysts, that is, Fe, Cu, Pd, Ag, and Au (Alfa Aesar, Pluratonic 99%+), were purchased in the form of 0.1 mm wires. Gallium (Sigma-Aldrich, 99% +) was coated on inert glass capillaries and loaded in the reactor. The mass of the catalyst loaded was 1 g for all catalysts. The reaction products were bubbled into deionized water, which was titrated with dilute sulfuric acid with phenolphthalein as indicator. The reactor was uniquely designed for ammonia synthesis by adding an online Agilent 7820A gas chromatograph (GC), equipped with a gas sampling valve and HP-PlotQ column (30 m × 0.32 mm × 20 μm). The gases were analyzed every 3 min for 30 min using the GC. All experiments were repeated thrice. The experiments were performed for input powers varying from 50 to 300 W at steps of 50 W. The plasma intensity (length of glow region) increased about 5 cm with increasing temperature from room temperature (25 °C) to 400 °C, suggesting that the addition of thermal energy to the plasma state helps in retaining the ionized state for longer lengths, that is, higher radical lifetime as the plasma zone has become longer, but the residence time of 0.72 s is assumed to be constant, as the vacuum pump works at constant power. Plasma power is the power delivered to the incoming gas.

Ammonia yield (%) is defined as the percentage of nitrogen molecules converted to ammonia. Because we work at reduced pressure, the energy cost associated with the vacuum pump must also be accounted for. The power consumed by the vacuum pump was calculated using a digital clamp on meter. The power read was 169 W which is 20% (approximately) of the total power consumed in the operation (RF Power Supply + Vacuum Pump) at 300 W output plasma power.

The energy yield is defined as the synthesis rate of ammonia per unit energy, while the energy cost is defined as the energy input for synthesis for one mole of ammonia. The formulas for calculating the energy yield and energy cost are as below. The electrical efficiency of the power supply is assumed to be 50% (average of 40−60%).

$$\text{energy yield} = \frac{\text{ammonia flow rate}}{\text{input power}} \tag{1}$$

where

$$\text{input power} = \frac{\text{plasma power}}{\text{electrical efficiency}} \tag{2}$$

For the energy yield in g-NH_3/kWh and energy cost in MJ/mol, we use the following equations and conversion factors

$$y\left(\frac{\text{g-NH}_3}{\text{h}}\right) = x\ (\text{sccm}) \times 7.435 \times 10^{-4} \times^{*} M_{NH_3} \times \frac{3600}{1000} \tag{3}$$

$$z\left(\frac{\text{g-NH}_3}{\text{kWh}}\right) = y\left(\frac{\text{g-NH}_3}{\text{h}}\right) \times \frac{1}{\text{input power (kW)}} \tag{4}$$

$$\text{energy cost}\left(\frac{\text{MJ}}{\text{mol}}\right) = \frac{17 \times 3.6}{z \times 0.5} \tag{5}$$

where x = flow rate of formed NH_3 in sccm, y = energy yield in g-NH_3/h, z = energy yield in g-NH_3/kWh, molar mass of ammonia = 17 g/mol, 1 kWh = 3.6 MJ, electrical efficiency of power supply = 0.5, 1 h = 3600 s, 1 g = 1000 mg, 1 sccm = 7.45 × 10^{-4} mmol/s. All conversion factors are obtained from the NIST database.[48]

Chemical Kinetics Model for Radio Frequency Plasma Ammonia Synthesis. A zero-dimensional chemical kinetics model was used to understand the important intermediate species and chemical pathways in plasma catalytic ammonia production by low pressure RF plasma. A set of time-dependent coupled differential equations accounts for the different reactions taking place in the plasma glow and at the reactor walls. The solution of the system of equations, which describes the time evolution of the various species from plasma ignition until the residence time is reached, is implemented in the ZDPlaskin code,[49] to elucidate the plasma chemistry. This model calculates the species densities as a function of time by means of continuity equations, taking into account the various production and loss terms:

$$\frac{dn_i}{dt} = \sum_j \left\{ (a_{ij}^{(2)} - a_{ij}^{(1)}) k_j \prod_l n_l^{a_{lj}^{(1)}} \right\} \tag{6}$$

where $a_{ij}^{(1)}$ and $a_{ij}^{(2)}$ are the stoichiometric coefficients of species i, at the left and right-hand side of a reaction j, respectively, n_l is the species density at the left-hand side of the reaction, and k_j is the rate coefficient of reaction j (see below).

The species considered in this model are listed in Table 1. The model considers 30 different species, including the electrons, various neutral species and ions, as well as 4 surface-adsorbed species, that is, N(s), H(s), NH(s), and NH_2(s), which are found to be the main precursors for ammonia synthesis. Adsorbed NH_3 molecules are assumed to be desorbed spontaneously following Carrasco et al.,[50] so that NH_3(s) is not separately defined.

The different chemical reactions included in the model are based on Carrasco et al.[50] but many other reactions have been added, involving the electronically excited molecules and atoms, as well as more gas phase reactions, which gradually become important with rising operating pressure. The gas phase reactions considered are electron impact ionization, excitation and dissociation of various neutral species, electron−ion recombination, ion−molecule reactions, as well as neutral species reactions (see Tables S3−S6). The surface reactions comprise ion neutralization and wall relaxation of excited molecules at the reactor walls, as well as heterogeneous reactions of the neutral species (see Tables S7−S9). In the work of Carrasco et al.,[50] the electrons are assumed to follow a Maxwellian-like energy distribution and the rate coefficients of electron impact reactions are fitted as a function of electron temperature. However, deviations from a Maxwellian behavior often take place in the discharge and therefore, we use the original cross sections to directly calculate the rate coefficients of the electron impact reactions. Although the vibration-

DOI: 10.1021/acsaem.8b00898
ACS Appl. Energy Mater. 2018, 1, 4824−4839

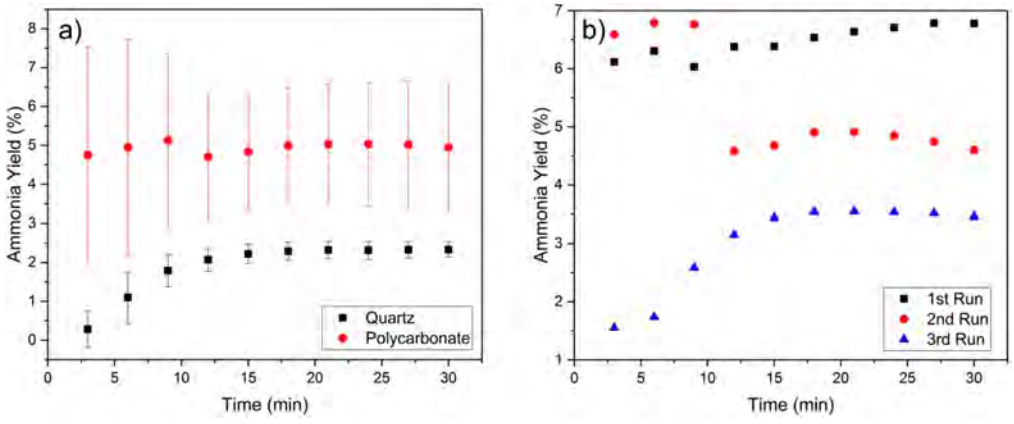

Figure 2. Ammonia yield (%) versus time (min) (a) for quartz and polycarbonate tube and (b) for various runs on polycarbonate tube.

ally excited molecules are not explicitly included in our model, electron impact vibrational excitation is included to describe the electron energy loss processes and hence to accurately calculate the electron energy distribution function (EEDF).

The production of NH_3 is assumed to take place by the successive hydrogenation of adsorbed N atoms and N-containing radicals at the surface of the quartz tube and the metal catalyst in the furnace. In fact, our model reveals that the gas phase volume reactions alone are not able to produce ammonia in detectable amounts, in agreement with previous works.[50] To prove that surface reactions at the quartz tube (i.e., reactor wall) also contribute to ammonia production, we performed experiments at 150 W and room temperature, employing quartz and polycarbonate tubes. The average ammonia yield obtained when using quartz and polycarbonate was 2.3% and 4.9%, respectively, after 30 min of reaction (Figure 2a). This confirms that the reactor tube wall affects the ammonia production. As the polycarbonate tube was not stable after the second run (Figure 2b), all experiments were run in a quartz tube.

However, for the model, the effective surface area A should be known with taking into surface roughness into account. The discharge length and inner radius of the tube are defined as L and R, with L equal to 83 cm and R equal to 22 mm Hence, we can obtain the discharge volume and the inner geometric surface area of the quartz tube as $V = \pi R^2 L$ and $A = 2\pi RL$, respectively. As noted by Kim et al.,[52] the surface roughness factor can vary a lot, depending on the surface conditions and measurement method. Bikerman reported that the surface roughness of glass varies between 1.6 and 5.4.[53] To estimate the effective surface area A in our model, we assumed a surface roughness factor of 2. This is in between the value of 2.4, adopted by Gordiets et al.,[39] and the value of 1.6, obtained by Carolus et al.[54] Hence, we assume the ratio of reactor volume to active catalyst surface area, $V/A = (\pi R^2 L)/(\xi 2\pi RL) = R/2/\xi = R/4 = 0.275$ cm, when a surface roughness factor $\xi = 2$ is assumed. To investigate the influence of this parameter on the calculated NH_3 yields, we performed calculations for various values of $\xi = 1$, 2, 3, and 5, at a discharge power of 150 W. We can see from Figure 3 that with increasing value of the surface roughness factor, the calculated NH_3 yield gradually increases, indicating the significant role of surface reactions in determining the NH_3 yield.

The rate coefficients for the neutralization of ions (K1−K10 in Table S7) at the walls (i.e., both quartz tube and Fe catalyst) are obtained by considering that the net ion generation in the gas phase (i.e., difference between the total ion density produced by electron impact ionization (X17−X28) and destroyed by electron−ion recombination (E1−E12)) must be balanced by the total ion flux to the walls to meet the electroneutrality condition.[50]

$$k_i = \frac{\sum_j R_j^X - \sum_k R_k^E}{\sqrt{m_i}\left(\sum_{10}^{l=1} \frac{[z_l]}{\sqrt{m_l}}\right)} \quad (7)$$

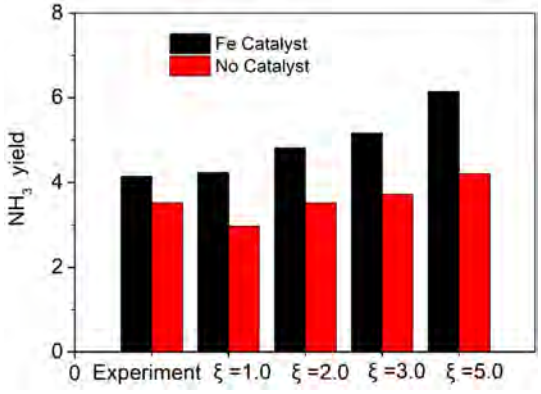

Figure 3. Experimental and calculated ammonia yields without catalyst and with Fe catalyst for a discharge power of 150 W, assuming different values for the surface roughness factor.

where $[z_l]$ is the density of the ionic species and R_j^X and R_k^E are the rates of electron impact ionization and electron−ion recombination, respectively. The loss rate of a given ion to the walls is proportional to its mobility, and thus inversely proportional to the square root of its mass $\sqrt{m_l}$.

The rate coefficients for relaxation reactions of the electronically excited states of N_2 and H_2 upon interaction with a surface (i.e., both quartz tube and Fe catalyst), that is, reactions W1−W6 in Table S8, are calculated using Chantry's formula.[55]

$$k_{\text{wall}} = \left(\frac{\Lambda^2}{D} + \frac{V}{A}\frac{2(2-\gamma_{\text{wall}})}{\bar{\nu}\gamma_{\text{wall}}}\right)^{-1} \quad (8)$$

Λ indicates the diffusion length, which is defined from the radius R of the reactor, using $R/2.405$ when Fe catalyst is not loaded. When Fe catalyst is loaded, we use $\Lambda = 0.2 \times R/2.405$, considering the reduced gap. D is the diffusion coefficient, $\bar{\nu}$ is the thermal velocity of the excited molecules, and V/A is the ratio of volume to inner surface area of the reactor. The wall loss probability γ_{wall} of the electronically excited states of N_2 was assumed to be the same as used by Gordiets et al.[56] The same estimate was used for electronically excited H_2 molecules, following the work of Hong et al.[51] Hence, we assume $\gamma_{\text{wall}} = 10^{-3}$ for all excited molecules. Note that this rate coefficient takes into account the decay rate of the species due to loss by diffusion in the discharge volume, as well as the surface interactions with the wall, which correspond to the first and second terms in eq S2, respectively.

Heterogeneous plasma−surface interactions can be broken down into (1) adsorption, (2) surface diffusion, (3) E−R (Eley−Rideal) interactions between surface-adsorbed and gas-phase species, (4) L−H (Langmuir−Hinshelwood) interactions between two surface-adsorbed species, and (5) desorption. For the heterogeneous

DOI: 10.1021/acsaem.8b00898
ACS Appl. Energy Mater. 2018, 1, 4824−4839

reactions in our model at both the quartz wall of the reactor and the Fe catalyst, we have introduced some general approximations: (i) the adsorption follows Langmuir theory, that is, gas phase species can only adsorb on free surface sites until the surface is fully covered by adsorbates (monolayer adsorption), (ii) all the surface sites are treated as identical, and (iii) the adsorbate−adsorbate interactions are neglected. We do not consider surface modifications or solubility of gases in the bulk surface to be of relevance for the kinetics of ammonia production. This assumption is based on surface science studies and high-pressure catalysis modeling.[57] When the product of E−R or L−H interactions is a stable N_2, H_2 or NH_3 molecule, it will be desorbed back to the gas phase; otherwise it is assumed to remain on the surface as an intermediate surface-adsorbed species, that is, NH_x(s) (with x = 1 or 2), N(s) or H(s). Hence, spontaneous desorption of N, H and NH_x radicals is not included in the model, following Carrasco et al.[50] and Hong et al.[51]

We consider two types of surfaces in the model: a quartz surface (reactor tube), and a surface of intermediate properties, which mimics in our 0D model the two-stage reactor used in our experiments when Fe catalyst is loaded in the furnace. The reaction rate coefficients of the surface with intermediate properties are obtained from the corresponding data for quartz and Fe catalyst, as explained below. We need reaction probabilities and reaction energies (activation energy and diffusion energy, see below) to determine the rate coefficients of the heterogeneous reactions, both at the quartz and Fe catalyst surface. The data of metallic Fe surfaces are most readily available[50] (see Table S9). When no catalyst is loaded in the furnace, the model considers reactions at the quartz surface, but the surface reaction coefficients for nonmetals are not well-known, hence we estimated them based on literature (see details below).

In all cases investigated, the quartz wall and Fe catalyst surface temperature was assumed to be equal to the gas temperature. Indeed, the surface reactions need a longer time to reach equilibrium, so there will be thorough heat transfer between the gas and the surfaces before the gas and surface-adsorbed species concentrations reach steady state.[51] In our 0D model, we converted the surface densities of all surface-adsorbed species, as well as of the free surface sites, both with units of cm^{-2}, to the equivalent volumetric densities with units of cm^{-3}, by dividing by the ratio of volume to inner surface area of the reactor, V/A. Similarly, we converted the surface reaction coefficients (in $cm^2\ s^{-1}$) to the equivalent volumetric reaction coefficients (in $cm^3\ s^{-1}$) by multiplying by V/A. Finally, even when the surface reactions are included in the model, the partial pressure of the gaseous species was kept constant during the simulation. This is justified, because the experiments are operated at constant pressure.

When N, H, and NH_x radicals from the discharge interact with the (quartz or catalyst) surface, they will adsorb (reactions S1−S4), with an adsorption coefficient k_{ads}, of which the value depends on the surface properties and is calculated with a similar formula as for surface relaxation by excited molecules (cf., above)

$$k_{ads} = \left(\frac{\Lambda^2}{D} + \frac{V}{A} \frac{2(2 - \gamma_{ads})}{\bar{v}\gamma_{ads}} \right)^{-1} {S_T}^{-1} \tag{9}$$

where S_T is the total surface site density, which is assumed to be 10^{15} cm^{-2}[58] following the recommendation by Carrasco et al.,[50] γ_{ads} is the adsorption probability (called in general reaction probability in Table S9), and the other symbols have been explained above.

H_2 and N_2 can be formed by recombination-surface desorption reactions. In principle, both Eley−Rideal (E-R) and Langmuir−Hinshelwood (L-H) mechanisms are possible. In our work, we only include the E-R mechanism between surface-adsorbed N(s) and H(s) and gas-phase N and H, as presented in Table S9 (reactions S5−S6) because of the low contribution of the L−H interaction in H_2 recombination[59] and the high activation barrier for diffusion of N(s) atoms.[60] The rate coefficient of this process, k_{ER}, is calculated with eq 9, with γ_{ads} replaced by the E-R reaction probability γ_{ER}, presented in Table S9.

The surface adsorption and recombination-desorption on clean metallic surfaces is better understood than on nonmetal surfaces. The initial adsorption or sticking probabilities of atoms and radicals on a clean metallic surface are often taken to be 1 because of their high reactivity.[61] Therefore, the measured total surface loss probability (sometimes referred to as the total recombination probability) from literature can be assigned as the E−R recombination probability γ_{ER} for metallic surfaces. The values of γ_{ads} for N, H, and NH_x radicals, set equal to 1, and the E−R recombination probabilities γ_{ER} for the adsorbed species with gas phase species on metallic surfaces (see Table S9) were taken from Carrasco et al.[50] The total surface loss and surface recombination probabilities for nonmetals are not well-known, apart from a few semiconductor materials, such as Si and GaAs.[62] Indeed, these probabilities are influenced by the type of species, the gas composition, the plasma characteristics and the operating pressure, as well as by the surface properties, including the surface temperature, chemical composition, surface functional groups formed by pretreatment, crystalline structure, and morphology.[63] Hence, both the total surface loss and its distribution between surface adsorption and E-R recombination probabilities requires to make some assumptions. We assume the reaction probabilities for direct adsorption of N atoms (reactions S1), and for recombination-desorption of N and H atoms into N_2 and H_2 (reactions S5 and S6) on silica to be a factor 0.18 lower than on a metallic surface, while the reaction probabilities for direct adsorption of H atoms and NH and NH_2 radicals (reactions S2−S4) are assumed to be a factor 0.018 lower, hence yielding the values listed in Table S9. Note that the assumed reaction probability for direct adsorption of H atoms on a silica surface is thus 1 order of magnitude lower than for N atoms, in agreement with Hong et al.[51] Indeed, a higher value for the H atoms would yield a large overestimation of the coverage of H(s) and an underestimation of N(s) on the surface. The latter would produce a lower estimate of the ammonia yield than in the experiments. By multiplying the above-mentioned reaction probabilities for direct adsorption and recombination-desorption for N and H atoms on silica, we obtain total surface loss probabilities $\gamma = 1.9 \times 10^{-4}$ for N and $\gamma = 4.9 \times 10^{-6}$ for H. The former value is within the literature range noted by Kim and Boudart,[52] which varies between 2×10^{-6} and 2×10^{-4}. The latter is also reasonable, because an order of magnitude lower total surface loss probability of H than for N on a silica-like surface was also reported from the measurements of Kim and Boudart.[52] Furthermore, these values give good agreement with the measured ammonia yields.

The reaction rate coefficients of other E-R (reactions S7−S13) producing adsorbed NH_x(s) radicals and gaseous NH_3 molecules are determined in the same way with formula (reaction S3). We followed Carrasco et al. for the reaction probabilities of NH_x(s) or NH_3 formation on metal surfaces, and in the absence of published data, we made the same assumptions as above for nonmetallic surfaces, as shown in Table S9. Indeed, for consistency with our estimates for surface recombination-desorption, the probabilities for the E-R (reactions S7−S13) on a silica surface were assumed to be a factor 0.18 lower than on metallic surfaces, which yields values in the same order as estimated by Hong et al. for an alumina surface.[51]

The rate coefficients of the Langmuir−Hinshelwood reactions between surface-adsorbed species (reactions S14−S16) are calculated by

$$k_{LH} = \frac{\nu}{4S_T} \exp\left(-\frac{E_a + E_d}{k_B T_{wall}} \right) \tag{10}$$

where ν is the surface diffusional jump frequency, which was approximated as $\sim 10^{13}\ s^{-1}$, following the assumption of Carrasco et al.[50] E_d indicates the diffusion energy barrier, for which we adopt a value of 0.2 eV for metal surfaces, following the recommendation by Gordiets et al.,[56] and in the absence of data, we use a higher value of 0.5 eV for quartz (see Table S9). The activation energies E_a for the specific L-H interactions are also given in Table S9 (assumed to be the same for quartz and Fe catalyst), and they were adopted from Carrasco et al.,[50] whose values are compatible with the studies of Ertl et al.[60] on chemisorbed species.

DOI: 10.1021/acsaem.8b00898
ACS Appl. Energy Mater. 2018, 1, 4824−4839

Finally, in addition to direct adsorption of atoms or radicals (cf., above), we also include dissociative adsorption of molecules (either in ground state or electronically excited levels) (reactions S17−S20). Upon increasing pressure, dissociative adsorption may play a more important role, just like three-body reactions in the gas phase, so they are included in our model, although these processes turn out to be almost negligible at the pressure under study here (0.26 Torr). The rate coefficients of dissociative adsorption of molecules are calculated as

$$k_{\mathrm{dad}} = \left(\frac{\Lambda^2}{D} + \frac{V}{A} \frac{2(2-\gamma_{\mathrm{dad}})}{\bar{v}\gamma_{\mathrm{dad}}} \right)^{-1} S_{\mathrm{T}}{}^{-2} \tag{11}$$

Note the difference with eq 9, that is, $S_{\mathrm{T}}{}^{-1}$ for adsorption versus $S_{\mathrm{T}}{}^{-2}$ for dissociative adsorption, as the latter requires two surface sites. γ_{dad} is the reaction probability for dissociative adsorption of molecules. For the ground state N_2 molecules, we calculated γ_{dad} following Hansen et al.[64,65] The value greatly depends on the vibrational state, as well as on the collision energy. We used an analytic representation of the calculated dissociative sticking probability by Rettner et al.,[66] which gives a value of 8.20×10^{-7} for a metallic surface (see Table S9). This low value makes that dissociative adsorption by N_2 molecules is virtually negligible.

The reaction probabilities for ground state H_2 molecules, as well as for the electronically excited states of N_2 and H_2 are calculated following the recommendation of Hong et al.,[51] and they are listed in Table S9 for the Fe catalyst surface. Again, we assume the probabilities for dissociative adsorption on a silica surface to be a factor 0.18 lower than on metallic surfaces (see Table S9).

As mentioned above, when Fe catalyst is loaded in the furnace, we have to use effective reaction probabilities, being a combination of the corresponding values for quartz and Fe catalyst, considering the relative contribution from the quartz surface and the Fe catalyst

$$\gamma_{\mathrm{eff}} = \gamma_{\mathrm{quartz}} \times \frac{l_{\mathrm{quartz}}}{l_{\mathrm{plasma}}} + \gamma_{\mathrm{catalyst}} \times \frac{l_{\mathrm{catalyst}}}{l_{\mathrm{plasma}}} \tag{12}$$

where γ_{quartz} and $\gamma_{\mathrm{catalyst}}$ are the reaction probabilities for a pure quartz surface and pure Fe catalyst, respectively (as listed in Table S9). l_{quartz}, l_{catalyst}, and $l_{\mathrm{plasma}} = l_{\mathrm{quartz}} + l_{\mathrm{catalyst}}$ are the lengths of the quartz tube surface and of the Fe catalyst in the discharge plasma, as well as the total plasma length observed by the experiments.

Equation 12 is used for all reactions in Table S9, except for reactions S2−S4 and reactions S14−S16. Indeed, as mentioned above, the reaction probabilities for reactions S2−S4 on silica are 1 order of magnitude lower than for direct adsorption of N (reaction S1). When Fe catalyst is loaded in the furnace, the effective adsorption probability calculated by eq 12 is highly overestimated, leading to an unrealistic (too low) ammonia yield, because the surfaces sites are almost completely occupied by H(s), which greatly prohibits the adsorption of N-containing species and hence the ammonia synthesis.[67] As a result, we used the following relationship instead, to predict the effective reaction probabilities for the reactions S2−S4.

$$\frac{1}{\gamma_{\mathrm{eff}}} = \frac{1}{\gamma_{\mathrm{quartz}}} \times \frac{l_{\mathrm{quartz}}}{l_{\mathrm{plasma}}} + \frac{1}{\gamma_{\mathrm{catalyst}}} \times \frac{l_{\mathrm{catalyst}}}{l_{\mathrm{plasma}}} \tag{13}$$

Furthermore, for the L-H reactions S14−S16, we assume a constant activation energy for different surfaces conditions (cf., above), but the diffusion energy barriers for different surfaces conditions are approximated with the following expression.

$$E_{\mathrm{deff}} = E_{\mathrm{dquartz}} \times \frac{l_{\mathrm{quartz}}}{l_{\mathrm{plasma}}} + E_{\mathrm{dcatalyst}} \times \frac{l_{\mathrm{catalyst}}}{l_{\mathrm{plasma}}} \tag{14}$$

where E_{dquartz} and $E_{\mathrm{dcatalyst}}$ are the diffusion energy barriers for quartz and Fe catalyst.

In literature, three different mechanisms of N_2 splitting in plasma-based ammonia synthesis are reported. Matsumoto et al. proposed the dissociative adsorption of electronically excited N_2 molecules as the dominant channel for N_2 splitting in a low pressure RF-discharge.[31,33,45] Hong et al. included both the plasma kinetics and plasma-catalyst interactions and theoretically proposed that direct electron impact dissociation of N_2 into N atoms dominates in N_2 splitting for atmospheric pressure DBD.[57] Carrasco et al. also presented a similar mechanism by combined theoretical and experimental investigation in low pressure DC plasmas, although their simulation did not take into account the possible influence of electronically excited states of N_2.[39,56] On the basis of a density-functional-theory-based microkinetic model, Mehta et al. showed the significant role of vibrationally excited N_2 states in the dissociative adsorption of N_2 molecules for an atmospheric-pressure DBD, assuming that the N_2 vibrationally excited states follow the Treanor distribution, but no plasma chemistry was included in their model.[68] Thus, on the basis of these models, the three different mechanisms that have been proposed are (i) dissociative adsorption of electronically excited N_2 molecules, (ii) direct electron impact dissociation of N_2 in the plasma, and (iii) dissociative adsorption of vibrationally excited N_2 molecules. In our model, we took into account the first and second mechanism, as the third mechanism can be neglected in this low-pressure RF plasma, because it is characterized by too high electron temperature to populate the N_2 vibrational levels. To evaluate the importance of the first mechanism, we have taken into account several electronically excited levels of N_2 (and H_2) in our model (see Table 3), but our simulations reveal that they are of minor importance for ammonia synthesis at our conditions (see Underlying Mechanisms section below).

RESULTS AND DISCUSSION

Plasma-Based Ammonia Synthesis without Catalyst.

Figure 4 shows the ammonia yield as a function of time, for various input powers, without catalyst at 400 °C and 0.26 Torr. As the RF power is delivered through a coaxial cable, some of the power is reflected; in our case this reflected power is less than 5%, hence the input power is taken as the plasma power. The input power for plasma generation plays an important role in achieving the final yield at equilibrium, since typically a higher yield is obtained at higher power. In our case, plasma power saturation is observed above 150−200 W. Furthermore, no other peaks than ammonia were observed in the gas chromatogram (GC), suggesting that no hydrazine was produced for uncatalyzed RF plasma assisted ammonia synthesis. The maximum yield of 3.75% was achieved at 200−300 W, after 12 min. This indicates that after 12 min of

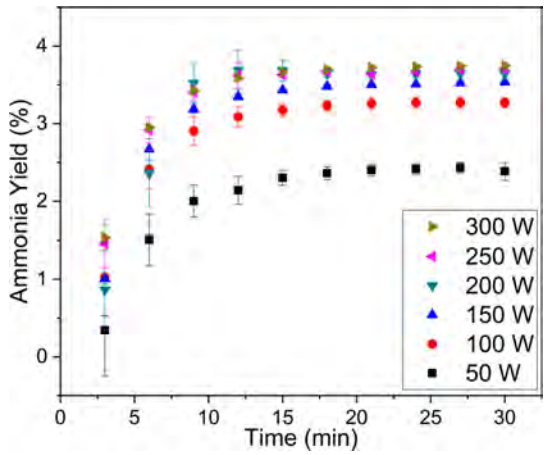

Figure 4. Ammonia yield (%) vs time for various plasma powers (W) without catalyst at 400 °C and 0.26 Torr.

DOI: 10.1021/acsaem.8b00898
ACS Appl. Energy Mater. 2018, 1, 4824−4839

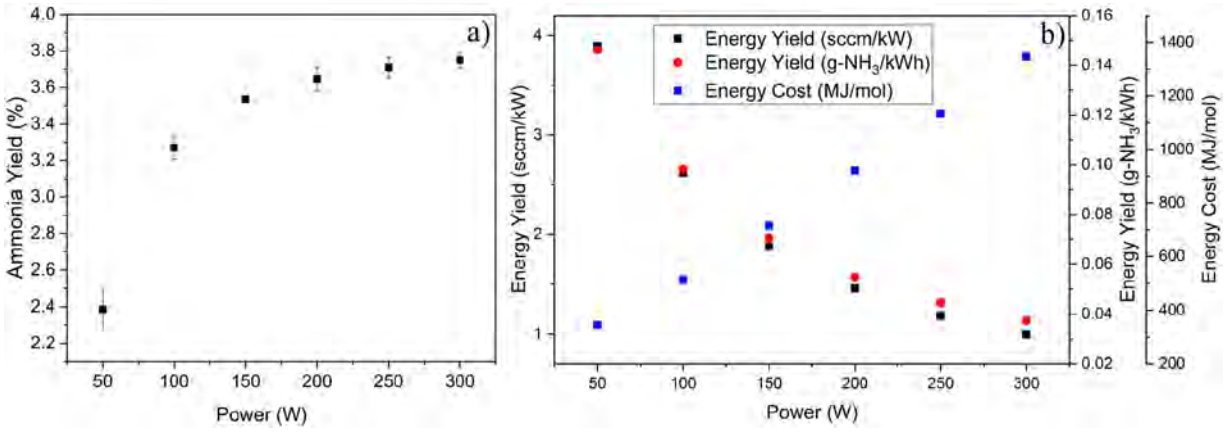

Figure 5. (a) Ammonia yield (%) and (b) energy yield (both in sccm/kW and g-NH_3/kWh) and energy cost (MJ/mol) versus power (W).

plasma initiation, the generation of excited species and radicals reaches equilibrium, leading to a constant yield hereafter.

The plasma glow region length increases with power from 50 to 300 W (Figure S1). Increasing power outcomes in higher concentration of energized species. Higher power would naively seem to suggest a higher concentration of excited species or species of higher mean energy. This increases the probability of successful collisions between radicals, explaining the higher yield at high power. Indeed, we suggest that the ammonia production occurs in the excitation (glow) region. This was confirmed by running a reaction at 25 °C (room temperature) with plasma turned on, which yielded an ammonia yield of 3.14% at 300 W; hence it is clearly a plasma effect and not a thermal effect that is responsible for the bond breakage. It is important to mention that even at temperatures as high as 400 °C, no ammonia was detected in the absence of plasma, which resonates with the fact that thermal energy is not enough to break the nitrogen triple bond. The standard deviation of the trails after the reaction reached steady state was less than 2% in all cases, except for 50 W, where it was 5%.

The change in final (steady-state) ammonia yield with respect to plasma power is shown in Figure 5a. As power increases, the yield also increases. The energy yield and energy cost are shown in Figure 5b. For calculation purposes, the electrical efficiency of the RF power supply is taken to be 50%, while the real efficiency varies from 40 to 60%,[69,70] with higher efficiency as the input power increases. In general, the energy yield drops upon increasing power because the ammonia yield increases less than linearly with power, so the extra power is not entirely used to dissociate extra N_2 molecules. This has been also observed in some other plasma mediated processes, such as CO_2 splitting and DRM.[71] For the same reason, the energy cost rises nearly linearly with increasing power. Without catalyst at 50 W and 400 °C the highest energy yield achieved was 3.9 sccm/kW, or 0.14 g-NH_3/kWh, corresponding to an energy cost of 351 MJ/mol. However, this condition gives the lowest ammonia yield. Vice versa, the highest power gives the highest ammonia yield, but the lowest energy yield and highest energy cost. Several reports, state that the ammonia yield will decrease quadratically with increase in flow rate whereas the energy yield increases quadratically with increase in total mass flow rate. Or in other words, the energy yield increases, and ammonia yield, that is, nitrogen conversion decreases.[30,40,72−74]

Ammonia Synthesis by Plasma Catalysis. The catalysts were loaded in the furnace-plasma zone, in the form of a mesh for Fe, Cu, Pd, Au and Ag, and as metal coated on inert glass capillary tubes for Ga, since it is a liquid metal (Figure S2). The yield was monitored as described in the Experimental Section. The reaction conditions were 400 °C, and power values were 50, 150, and 300 W (Figure 6).

The ammonia yield is plotted against time for three different powers and different catalysts in Figure 6a, c, and e, while the steady-state ammonia yield is plotted against catalyst for the three powers in Figure 6b, d, and f. The plasma-catalytic activity increases with power, but the order of catalytic activity changes upon rising power.

When comparing the performance of the mesh catalysts with the molten Ga, we can see that the latter performs best at 150 W and is less efficient at 300 W. The main drive to use molten Ga is the reported existence of synergistic interactions of H_2 and N_2 plasmas with molten Ga. Indeed, Carreon et al.[75] reported that the nitrogen and hydrogen adsorption and desorption are highly dependent on the temperature and plasma power, suggesting the use of Ga as catalyst for this process at mild conditions.

The introduction of a catalyst does not change the trend of the curves as a function of plasma power, or the time needed to reach steady state. As can be observed at 50 W, the use of a catalyst made little difference comparing to the noncatalyzed reaction. This small difference could be due to the partial excitation and lower degree of ionization at low power. As there are only limited reactive species available to interact, the catalyst seems not to have a great impact. The best catalyst at this power was Ag followed by Ga. The ammonia yield increases from 2.4% (no catalyst) to 3.7% (Ag). The order of catalytic activity was Ag > Ga > Cu > Pd > Fe > Au.

The trend of catalytic activity changes drastically when the power rises to 150 and 300 W. At 150 W, the catalysts exhibit the following trend: Ga > Pd > Au > Ag > Cu > Fe. The yield increases from 3.5% (no catalyst) to 10.1% (Ga). For all the catalysts employed, the activity decreased after the first use but remained constant thereafter. The decay from first to second use was <5% for Cu, Au, Ag, and Ga, and ∼15% for Fe and Pd. Being so small we averaged the first, second and third runs, and this is the yield value reported. The spent catalysts are shown in Figures S3 and S4, indicating no color change, except for Ga at 300 W (see also below).

At 300 W, not only the catalytic activity has increased drastically, but also the catalytic trend changed considerably. The catalytic activity follows the order: Au > Ag > Pd > Cu > Ga > Fe. All noble metals used, that is, Pd, Ag, and Au,

DOI: 10.1021/acsaem.8b00898
ACS Appl. Energy Mater. 2018, 1, 4824−4839

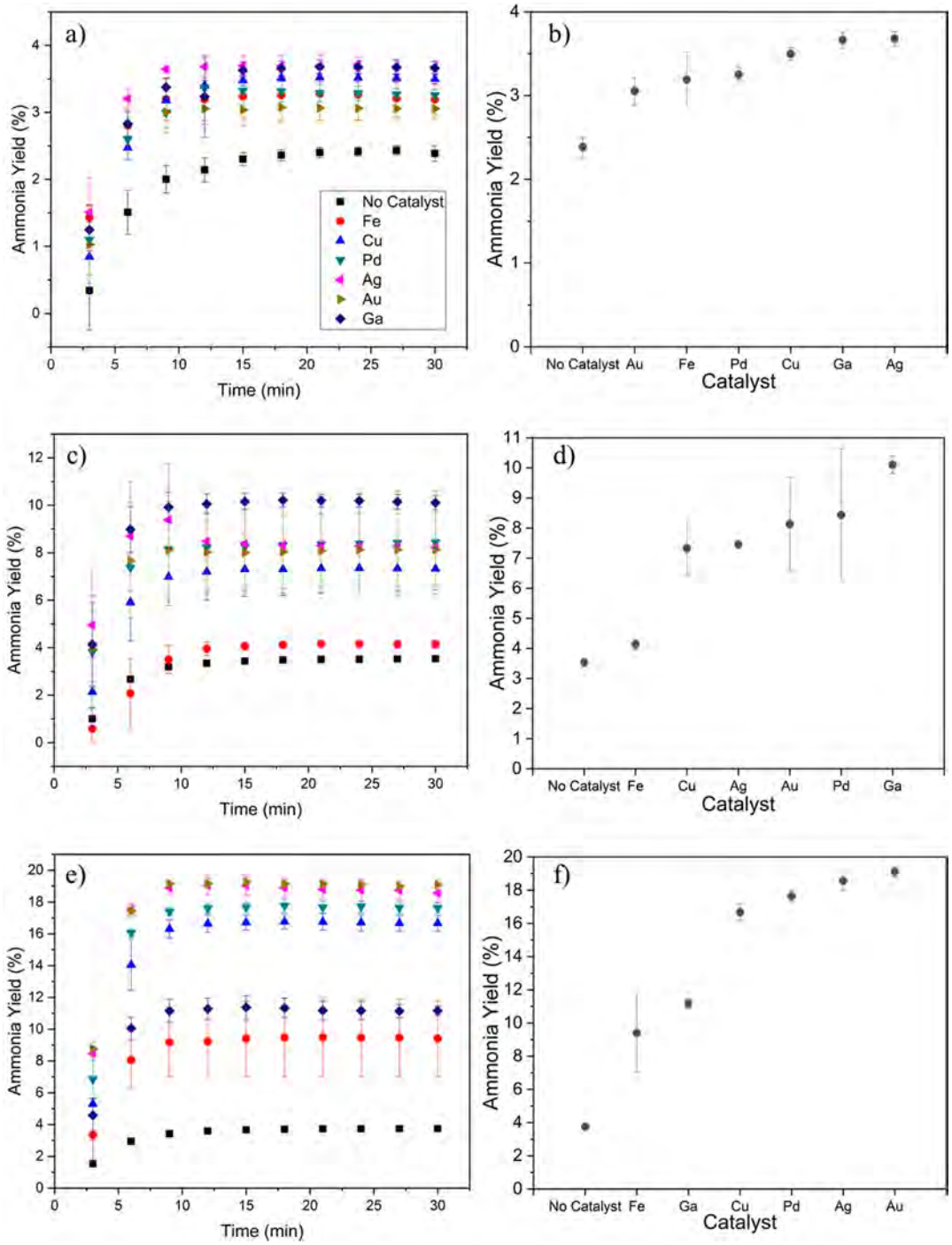

Figure 6. Ammonia yield (%) vs time at (a) 50, (c) 150, and (e) 300 W, for different catalyst materials, and ammonia yield (%) at 30 min, plotted for different catalysts at (b) 50, (d) 150, and (f) 300 W.

achieved a yield of ∼17−19%. It is worth mentioning that at 150 and 300 W, if we ignore the molten metal Ga, the order of catalytic activity is almost the same, that is, Au > Ag > Pd > Cu > Fe. The activity of Pd changed but was in the vicinity of Ag and Au.

Interestingly, the performance of Ga versus the other transition metals varied considerably from 150 to 300 W, which is because of its tendency to form stable nitrides at high temperatures. Indeed, Ga can interact with N_2 and H_2 plasma at low temperature and powers without forming a nitride, which was also confirmed by experiments.[75] At higher power, that is, 300 W, the activity of Ga toward ammonia formation is significantly reduced, which indicates that this molten metal can act as catalyst under certain (mild) conditions only.

Remarkably, the highest yield (19.1%) was obtained with Au as catalyst at 300 W and 400 °C, which is higher than the commercial Haber-Bosch process yield of 15%.[76] However, the Haber−Bosch process energy yield of 500 g-NH_3/kWh,[77] and the energy cost of 0.48 MJ/mol[78] greatly surpass the values of our best catalysts (Pd, Ag, and Au), which range in between 0.18 and 0.19 g NH_3/kWh and 264−285 MJ/mol for energy yield and cost, respectively (see detailed discussion in later

DOI: 10.1021/acsaem.8b00898
ACS Appl. Energy Mater. 2018, 1, 4824−4839

Table 2. Ammonia Yield and Energy Yield/Energy Cost, Obtained in Our Study, with Various Catalysts, as Well as without Catalyst at 300 W and Comparison with Other Plasma Processes Used for Ammonia Synthesis

plasma	year	catalyst	NH_3 yield (%)	energy yield (g-NH_3/kWh)[a]	energy cost (MJ/mol)[b]	ref
radio frequency	1993	iron wires		0.025	856.2	43
	2018	no catalyst	3.7	0.04	1343	this study
		gallium	11.2	0.11	451	
		iron mesh	11.8	0.12	428	
		copper mesh	16.7	0.17	302	
		palladium mesh	17.6	0.18	285	
		silver mesh	18.6	0.19	271	
		gold mesh	19.1	0.19	264	
DBD	2017	Ru over γ-Al_2O_3	1.4		32	1
	2017	$BaTiO_3$ beads or porous Ni catalyst	9		81	41
	2017	Ru-MCM-41	0.1	1.7	27	73
	2017	wool-like gold	4.72	4.45	93	85
	2017	PZT powder	7		408	40
	2016	wool-like copper	3.5	3.3	93	38
	2015	$BaTiO_3$/PZT	2.75	0.72	136	37
	2008	no catalyst	0.8	1		88
	2003 and 2008	MgO	0.63	1.83		30 and 88
pulsed	2017	Mg promoted ruthenium over alumina		35.7	1.71	47
AC	2017	Mg promoted ruthenium over alumina		9.8−11.5	5.32	47
microwave	2008	no Catalyst	0.00025	0.03		33

[a]For comparison purposes, the energy yield is calculated for the input power (see Supporting Information for the exact formula). [b]The energy cost in our study is calculated from the electrical power drawn by the power supply (see Supporting Information for the exact formula).

sections). These values are somewhat better than in case of no catalyst, where the best energy yield was found to be 0.14 g-NH_3/kWh, and the lowest energy cost was 351 MJ/mol (see previous section). See Tables 2 and 3 below for more details.

Table 3. Comparison of Haber−Bosch versus RF Plasma Process for Ammonia Synthesis

parameters	Haber−Bosch	RF Plasma
yield	8−15%	19.1%
energy yield (g-NH_3/kWh)	500	0.22
energy cost (MJ/mol)	0.48	229
setup	small scale not viable	small scale viable
plant size for economy	more than 100 ton/day needed	potential to be adaptable for small scale plants in combination with renewable electricity sources
temperature	450−600 °C	25−400 °C
pressure	150−350 bar	0.01 bar
limiting reaction	nitrogen dissociation	intermediate formation
catalyst	iron catalyst	gold catalyst
catalyst poisoning	catalyst needs to be regenerated	hydrogen plasma keeps the catalyst clean

Comparisons of Simulations and Experiments. Chemical kinetics computer simulations were performed for the same conditions as in the experiments, without catalyst and with Fe catalyst. Only Fe was considered as catalyst because of the availability of reaction rate coefficients for Fe surfaces in literature, while these data are not so well-known for the other metal catalysts. The calculated ammonia yields at different discharge powers are compared to the experimental values in Figure 7. Generally, good agreement is reached between the calculated and experimental yields, showing that the chemical kinetics model can provide a realistic picture of the plasma chemistry in RF plasma-based ammonia synthesis, and can be used to reveal the underlying mechanisms.

The experimental ammonia yields can only be reproduced if surface reactivity is taken into account, not only for the catalyst surface but also for the quartz tube. The latter is clearly demonstrated in the Supporting Information (SI). The physical and chemical properties of the wall or the catalyst significantly affect the synthesis process. To account for the surface reactivity in the simulations, we have applied reaction rate coefficients for Fe, adopted from literature, as well as for the quartz tube, based on the data for Fe and information from literature for silica-like glass and similar materials, to mimic the experiments without catalyst. For the two-stage plasma-catalytic reactor, we used reaction rate coefficients intermediate to the quartz tube and the pure Fe catalyst surface. Indeed, the Fe catalyst is not loaded in the excitation zone of the plasma, that is, the zone confined by the RF coils (see details in Figure 1). Hence, the plasma species interact with the quartz tube in the excitation stage, and with the Fe catalyst in the furnace stage of the reactor. To account for this in our 0D model, we use intermediate rate coefficients between quartz tube and Fe catalyst, defined by the length of the excitation and furnace stage (see SI for details).

If the heterogeneous plasma−surface interactions are ignored in the simulations, the gas volume reactions result in negligible ammonia synthesis because of the efficient electron impact dissociation of ammonia, which apparently exceeds the rate of the most important production process of ammonia, that is, through electron−ion recombination ($e^- + NH_4^+ \rightarrow NH_3 + H$ and $e^- + NH_3^+ \rightarrow NH_3$). However, when the surface reactions are included, the ammonia synthesis is triggered by the supply of atomic H and N to the surface (of the catalyst or simply the reactor walls), which depends on efficient dissociation of H_2 and N_2 in the plasma. The efficiency

DOI: 10.1021/acsaem.8b00898
ACS Appl. Energy Mater. 2018, 1, 4824−4839

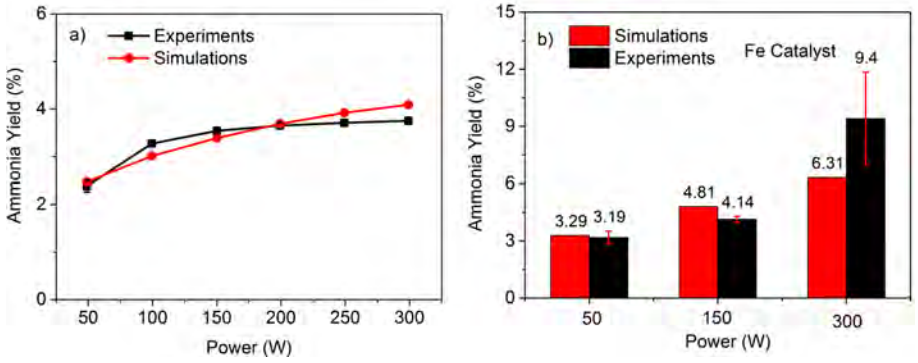

Figure 7. Experimental and calculated ammonia yields (a) without catalyst as a function of power and (b) with Fe catalyst for 3 different discharge powers, with experimental error bars.

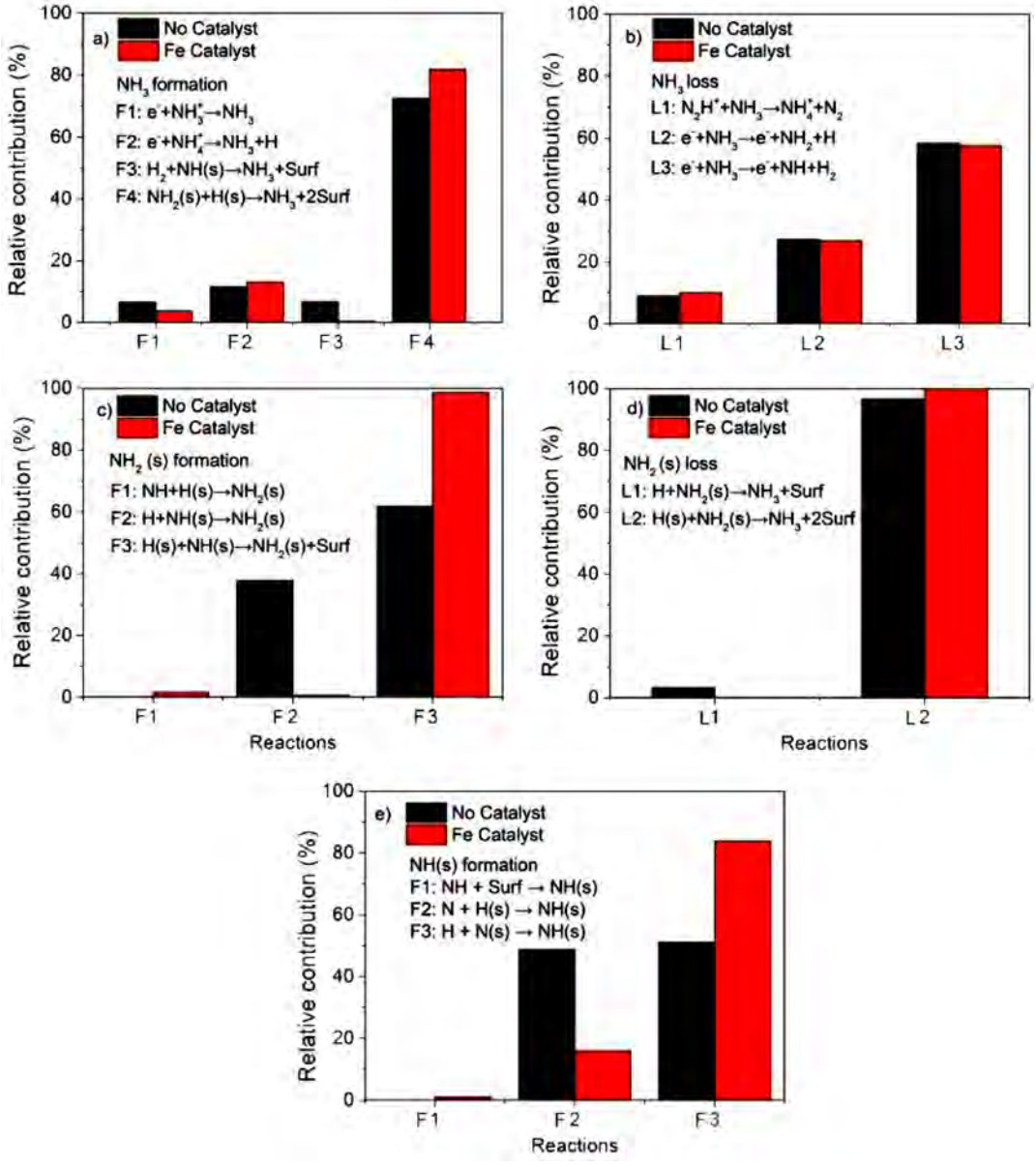

Figure 8. Relative contributions of the main processes leading to the (a) formation of NH_3, (b) loss of NH_3, (c) formation of $NH_2(s)$, (d) loss of $NH_2(s)$, and (e) formation of NH(s) for a plasma power of 150 W.

grows substantially with increasing power, both without and with catalyst. First, the rising discharge power enhances the electron temperature, and thus the rate of electron impact dissociation of H_2 and N_2, resulting in a more efficient supply

DOI: 10.1021/acsaem.8b00898
ACS Appl. Energy Mater. 2018, 1, 4824−4839

of atomic H and N to the surface. Second, the plasma glow region length increases, and thus, there is more overlap between the catalyst sector and the plasma, with rising plasma power. This leads to enhanced adsorption at the (catalyst or wall) surface and increased Eley−Rideal (E-R) recombination probabilities for N, H, and NH. In addition, the longer plasma glow region yields a longer residence time within the plasma. As a result, the ammonia yield from both simulations and experiments with and without catalyst increases with rising discharge power, as can be observed in Figure 7a and b.

Underlying Mechanisms. As the model gives good agreement with the experiments, we can use it to investigate the dominant reaction pathways for ammonia synthesis. This is illustrated in Figure 8, for the formation and loss of NH_3 (Figure 8a and b), $NH_2(s)$ (Figure 8c and 8d) and the formation of the important surface-adsorbed species NH(s) (Figure 8e) for a plasma power of 150 W, without and with Fe catalyst. This kinetic analysis was performed by looking at the time integrated rates of the various processes for the total residence time in the reactor.

As presented in Figure 8a and 8b, the gas volume reactions (i.e., electron−ion recombination: $e^- + NH_3^+ \rightarrow NH_3$ (F1) and $e^- + NH_4^+ \rightarrow NH_3 + H$ (F2)) are of minor importance for the formation of NH_3, with a relative contribution below 15%. The L−H interaction between H(s) and $NH_2(s)$ (F4) is the most important mechanism for ammonia production. The relative contributions are 73% and 82% without and with Fe catalyst, respectively. This indicates that ammonia is mostly formed at the surface of the reactor walls or the Fe catalyst by the successive hydrogenation of N atoms and N-containing radicals. The E−R interaction (F3) between NH(s) and H_2 from the gas phase also plays a role in the formation of NH_3 without catalyst, with a relative contribution of 6.8%, but it becomes negligible in case of the Fe catalyst. Our results support the prevalent view that L-H reactions are important for the heterogeneous synthesis of ammonia in low pressure discharge plasmas.[50]

The loss of NH_3 mainly results from electron impact dissociation into NH_2 and especially NH (reaction L2 and L3, respectively), which are equally important with and without Fe catalyst. These two reactions are also most important for NH_2 and NH formation. The contribution from other reactions is minor. It should be noted that, although it cannot be deduced from Figure 8, both the production and loss rates for NH_3 are higher with Fe catalyst because of the higher surface reactivity of the catalyst.

As $NH_2(s)$ is the most important precursor for ammonia synthesis (see Figure 8a), we present the relative contribution of the dominant formation and loss reactions of $NH_2(s)$ in Figure 8c and d. The predominant formation channel for $NH_2(s)$ is the L−H interaction between H(s) and NH(s) (F3), contributing for 62% and 98% without and with catalyst, respectively. The E−R interaction (F2) between NH(s) and H from the gas phase (F2: H + NH(s) → NH_2 (s)) is also important for the formation of $NH_2(s)$ without catalyst, with a relative contribution of 38%, but it becomes negligible in case of the Fe catalyst. This is because the higher surface reactivity of Fe yields a lower H atom density in the gas phase. Other reactions, such as direct adsorption of NH_2 on the surface, as well as the E-R interaction (F1: NH + H(s) → NH_2 (s)), contribute little to $NH_2(s)$ formation, because the densities of the gaseous reactants NH_2 and NH are small compared with the surface densities.

Without and with catalyst, the only dominant loss reaction of $NH_2(s)$ is the L-H reaction with H(s) (L2: H (s) + NH_2 (s) → NH_3), with a relative contribution of 97% and 99%, respectively. This is also the dominant formation reaction of NH_3, as shown in Figure 8a. The E-R reaction with H atoms (L1:H + NH_2 (s) → NH_3) is negligible, because of the lower density of H atoms in the gas phase compared with the surface density.

As NH(s) is the dominant precursor for $NH_2(s)$ (see Figure 8c), we present in Figure 8e the relative contributions of the main processes leading to the formation of NH(s). The most important formation reaction occurs between H and N(s) (F3), with a relative contribution of 51% and 84% without and with Fe catalyst, respectively. Furthermore, the E−R reaction between N atoms and H(s) (F2) is also an important formation process, but mainly without catalyst. Direct surface adsorption of NH radicals contributes little to NH(s) production because of the low density of gaseous NH species. Finally, nearly all loss of NH(s) is due to its reaction with H(s) producing $NH_2(s)$ (cf., Figure 8c) and is therefore not explicitly plotted in Figure 8.

General Overview of the Reaction Pathways. On the basis of the above analysis, we can compose a general picture of the dominant reaction pathways for RF plasma-based ammonia synthesis. This is summarized in Figure 9, for the case with Fe catalyst, in a 1:4 N_2/H_2 mixture, for a plasma power of 150 W and a pressure of 0.26 Torr.

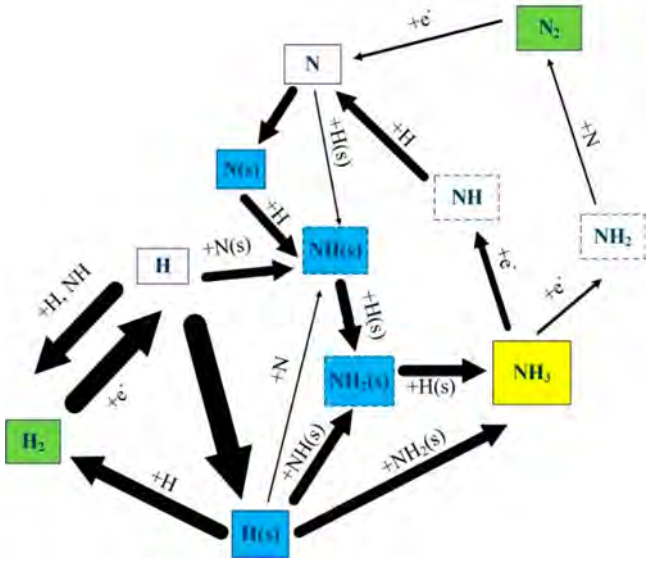

Figure 9. Schematic overview of the dominant reaction pathways for NH_3 synthesis with Fe catalyst, in a 1:4 N_2/H_2 mixture, for a plasma power of 150 W and a pressure of 0.26 Torr. The thickness of the arrow lines is proportional to the reaction rates.

The ammonia synthesis process starts with electron impact dissociation of N_2 and H_2, forming N and H atoms. The electron impact dissociation rate for H_2 is much larger than for N_2 because of a lower binding energy, leading to a much higher concentration of H atoms in the plasma. The H and N atoms can adsorb on free surface sites, to form H(s) and N(s). As the plasma conditions provide a higher H atom density in the gas phase, this leads to a preferentially H-covered surface, which forms not only NH_3 but also H_2. At the low pressure investigated here, electron impact dissociation of N_2, which is

DOI: 10.1021/acsaem.8b00898
ACS Appl. Energy Mater. 2018, 1, 4824−4839

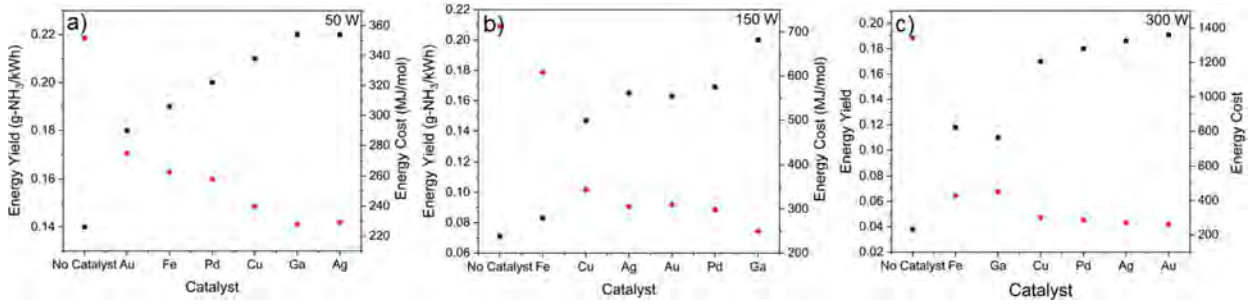

Figure 10. Energy yield (black) and energy cost (red) for different catalysts at different plasma power: (a) 50, (b) 150, and (c) 300 W.

controlled mainly by the electron temperature, supplies an adequate flux of N atoms to the surface (of the walls or catalyst) to favor hydrogenation of N(s), forming NH(s), followed by NH_2 (s), and hence promoting ammonia production. A feedback mechanism allows the formation of NH from NH_3, which is split in N and H_2 (upon collision with H atoms). These N atoms can also react with H(s) (N + H(s) → NH(s)), which competes with H_2 formation at the surface (by H + H(s) → H_2). NH(s) further reacts into NH_2(s), yielding again NH_3 formation. Our calculations reveal that the Langmuir−Hinshelwood (LH) mechanism predominantly contributes to the formation of NH_2(s) and NH_3 (i.e., upon reaction with H(s)), while the Eley−Rideal mechanism (upon collision with H atoms from the gas phase) only contributes for 0.30%. Finally, the dominant loss processes of NH_3 are electron impact dissociation, producing NH and NH_2 radicals.

To summarize, the RF plasma-based ammonia synthesis at low pressures (around 0.26 Torr) on Fe catalyst proceeds as follows:

1. $e^- + N_2 \rightarrow e^- + N + N$
2. $e^- + H_2 \rightarrow e^- + H + H$
3. $H + surf \rightarrow H(s)$
4. $N + surf \rightarrow N(s)$
5. $H + N(s) \rightarrow NH(s)$
6. $NH(s) + H(s) \rightarrow NH_2(s) + surf$
7. $NH_2(s) + H(s) \rightarrow NH_3 + 2surf$

It is important to note, however, that this proposed mechanism is pressure dependent. At higher pressure, some more reactions become important, more specifically some Eley−Rideal mechanisms, that is,

$$H + NH_2(s) \rightarrow NH_3$$

$$NH_2 + H(s) \rightarrow NH_3$$

$$H_2 + NH(s) \rightarrow NH_3$$

Indeed, these reactions become gradually more important with rising pressure because of the higher density of gaseous (plasma) species.

It should be mentioned that our model also includes the electronically excited states of N_2 and H_2, but our simulations reveal that the contribution of these excited species to the global chemistry of ammonia synthesis is small at the low pressures under study here and for the dimensions and characteristics of our reactor. Dissociative adsorption of electronically excited N_2 molecules at the surface (of the walls or catalyst) has a negligible contribution to N_2 splitting, because of their low concentration in the plasma. Indeed, the electronically excited states of N_2 can rapidly relax back to the ground state by fast quenching upon impact with neutral species and by radiative decay. The latter is confirmed by our optical emission spectroscopy measurements (see Figures S8 and S9). Furthermore, our measurements also provide evidence of atomic N emission at λ = 744.2 nm or λ = 746.8 nm, suggesting the dominance of N_2 splitting in the gas (plasma) phase.

Moreover, the operando optical emission spectroscopy measurements confirmed the interaction between the catalyst and the excited gas phase species, or the plasma catalytic effect. Indeed, when the H_α peak intensity increases, the ammonia yield decreases (see details in the SI). Specifically, the measurements indicate that the recombination of H atoms (related to the H_α peak, i.e., the most prominent hydrogen signature) on the metal catalyst surface reduces the available H atoms that can lead to the formation NH_x species, an essential step for ammonia synthesis. This experimental observation can be confirmed from the dominant reaction pathways obtained through our simulations (see Figure 9).

Ammonia Yield and Energy Yield/Energy Cost of Plasma Catalytic Ammonia Synthesis: Benchmarking with Literature. The energy yield and energy cost for all our experiments, that is, for the different power values and with the different catalysts, as well as without catalyst, are summarized in Figure 10. Opposite to the ammonia yield, the highest energy yields were mainly observed at 50 W. The highest energy yield is achieved when using Ga as catalyst at 50 W, reaching a value of 0.22 g-NH_3/kWh, which corresponds to an energy cost of 229 MJ/mol (see Figure 10a). The metal meshes follow the same trend for energy yield as for ammonia yield. The highest energy yield is obtained at 50 W, followed by 300 W. The lowest energy cost at 300 W is for Ag and Au, and reaches 270 MJ/mol. Despite the high ammonia yields achieved through RF plasma catalysis, that is, up to 19% (and thus higher than for the commercial Haber−Bosch process; cf above), the values for energy cost are 500 times higher than for the commercial Haber−Bosch process (0.48 MJ/mol). However, if comparing with other reports on RF low pressure plasmas, the energy yield has improved from 0.012 g-NH_3/kWh[43] to ∼0.2 g-NH_3/kWh in this work, depending on the power and catalyst used.

Table 2 lists the ammonia yields, energy yields, and energy costs obtained in our study, in comparison to the values reported in literature for plasma assisted ammonia synthesis in various types of plasma sources. The energy yield is described as the total ammonia output per energy input (see SI for detailed definition). This value highly depends on the input flow rate, which also governs the output flow rate of the products. In our study, the total flow rate is kept fixed at 20 sccm, yielding a quite low output flow rate in comparison with

DOI: 10.1021/acsaem.8b00898
ACS Appl. Energy Mater. 2018, 1, 4824−4839

the data reported in literature for other plasma reactors typically operating at atmospheric pressure, such as dielectric barrier discharges (DBDs), pulsed and AC plasmas. Indeed, typical experiments in DBD, pulsed or AC plasmas are carried out at a flow rate of ∼100 sccm, which is 5 times the flow rate used in our study.

On the other hand, in our case, the low pressure ensures uniformity of the reactants in contact with the catalytic surface inside the reaction chamber, leading to high gas conversion and high ammonia yields, compared to the other (higher pressure) plasma routes; see Table 2. Additionally, this uniformity can help us to understand the plasma-catalyst synergism. It is indeed our main objective to better understand this interaction, so that it can possibly be applied to other plasmas as well and can lead to further improvements. Finally, low pressure operation enables to keep the gas at room temperature, which is beneficial because ammonia synthesis is thermodynamically favored at low temperature, and the plasma accounts for activation of the reactants. Indeed, the atmospheric pressure microwave (MW) plasma[29] shows a much lower ammonia yield and energy yield than in our work (see Table 2), and gas quenching was pointed out in this case as the most effective technique to produce ammonia.[33] Indeed, microwave discharges at atmospheric pressure easily reach a gas temperature of several thousand Kelvin because of the rapid kinetic energy exchange between electrons and heavy particles.[79] In such case, the economics of thermal stabilization might be a technical barrier.

It should be realized that we have used simple catalysts in this work, to obtain a more basic insight of the underlying mechanisms. The employment of engineered catalysts, tailored to the plasma environment, will for sure lead to better energy yields. Moreover, we believe that the low energy yield in our case can be improved by scaling up the reactor to a considerable size, so that a higher flow rate can be used (cf., above). Upscaling of RF plasma reactors is certainly feasible, based on the large experience from the semiconductor industry.[80,81] Furthermore, among the advantages of RF sources, we should also mention that RF waves are categorized as nonionizing radiation, and their heating effect is less than for microwaves, which makes them less harmful in case of radiation leakage.[82] In addition, the RF coils are placed outside the plasma chamber, in contrast to other setups, like DBD, where the electrodes are inside the plasma chamber. Hence, they do not undergo plasma etching effects, so they can last longer[83] with no need to replace frequently, enhancing the lifetime of the plasma reactor.

It is important to mention that plasma catalysis is still at a very early stage, and there are still mainly unknowns, especially regarding the optimal conditions, the proper catalysts and the best plasma-catalyst pairs. However, a successful example, where plasma has shown its uniqueness, and which serves as motivation for the present work, is the plasma production of ozone. This process serves as a good example of a technique that, despite the limitation of the energy cost of ozone generation, is nowadays widely industrially applied after optimizations to reduce the energy cost.[84]

We can conclude from Table 2 that the ammonia yield and energy yield of plasma catalytic ammonia synthesis are in the range of 0.1−19% and 0.03−4.45 g-NH_3/kWh, respectively, with some exceptional cases for the energy yield (9.8−35.7 g-NH_3/kWh) for pulsed and AC plasmas, but no ammonia yields were reported in these cases. In general, the cost and recyclability of the catalyst impose a major challenge. Overall, very good results were obtained by Iwamoto et al.[85] who reported an ammonia yield of 4.72%, an energy yield of 4.45 g-NH_3/kWh and energy cost of 93 MJ/mol, when using atmospheric DBD plasma and wool-like Au catalyst. This yield is slightly higher than our yield of 3.75% without catalyst at 300 W and 400 °C. When we employ a Au mesh at 300 W and 400 °C, we obtain an unprecedented yield of 19.1%. However, Iwamoto's energy yield and energy cost are far superior compared to ours. Patil et al.[1] reported an even lower energy cost of 32 MJ/mol, when using Ru over γ-Al_2O_3 as catalyst in a DBD reactor, but their ammonia yield was only 1.4%. Kim et al.[47] obtained the highest energy yield of 35.7 g-NH_3/kWh and the lowest energy cost of 1.71 MJ/mol, when using a pulsed source and Ru(2) Mg(5)/γ-Al_2O_3 as catalyst, but they did not report the corresponding ammonia yield. However, one of the main drawbacks of their work is the employment of a catalyst which contains Ru, a metal even more expensive than Au. Furthermore, the yield of NH_3 obtained when using recycled catalyst was only half the value obtained when using fresh catalyst. The authors suggested that the presence of RuO_2 and metallic Ru benefits the NH_3 synthesis. However, because of the presence of highly reducing H radicals, the introduction of a small amount of O_2 was proposed to regenerate in situ the catalyst, which can lead to the formation of secondary subproducts and a complicated reaction pathway that can impact the reported values. This points out to the necessity of a proper catalyst selection, since recyclability and cost are critical parameters for potential industrial catalyst application.[86,87]

Benchmarking with the Haber−Bosch Process. It is immensely difficult and unfair to compare two different process occurring at different scales. The Haber-Bosch process occurs at industrial scale of 100 tons/day capacity whereas our process produces few grams of ammonia because of the scale of the reactor. Even though that is the case we have tried a crude attempt to compare them by using data from a somewhat scaled down (still in tons/day scale) Haber−Bosch process.

We already mentioned above that the maximum ammonia yield obtained in our work is higher than the values reported for the Haber−Bosch process, but our energy yield and energy cost are much worse, as presented in Table 3. The values are taken for the commercially viable Haber−Bosch process with lowest ammonia production capacity of 200 tons/day. It does not include the cost for hydrogen production.[3] This table also shows further differences in the setup and operating conditions of the Haber−Bosch process vs the RF plasma route, which can help to obtain a clear insight about this technology. In general, the proposed RF pathway has the main advantage of being viable at small scale viable, which is very promising in the future if combined with renewable electricity sources.[3] Furthermore, a lower temperature is employed due to the presence of reactive plasma species, which is thermodynamically more beneficial and results in an overall lower pressure process. Interestingly, the rate limiting step switches from N_2 dissociation in the Haber−Bosch process to NH_x formation in the RF plasma route, which clearly demonstrates the necessity of exploring potential new catalysts for this route.[3] Among the advantages of using plasma, the hydrogen plasma surface cleaning effect[89,90] is of great importance, since there should not be a problem of catalyst poisoning if a hydrocarbon is used as hydrogen source for this synthesis. This can be also partially supported by the fact that our catalysts retain their activity

DOI: 10.1021/acsaem.8b00898
ACS Appl. Energy Mater. 2018, 1, 4824−4839

fairly well after first use (Figure S4). We showed that Au is a promising catalyst, since it provided the best yield in our study. However, we employed metal meshes to determine the catalytic activity of the proposed metals and to obtain a more basic understanding, without focusing on engineering aspects. Nevertheless, there are still several material properties that still remain unexplored and that have the potential to enhance the catalytic activity and reduce the cost of the catalyst. Among these are the use of metal nanoparticles dispersed on high surface area supports, the use of molten alloys where the active phase (the expensive metal) is present in very small amount, and the use of porous materials that contain the active phase/metal in their structure. Therefore, we believe that there is still room for improvement for RF plasma-based ammonia synthesis.

CONCLUSIONS

Finding more efficient routes for ammonia synthesis has been a challenge for more than a century. Emerging technologies, like plasma catalysis, create some new opportunities in this direction. We explored the potential of RF plasma synthesis, both without and with metal catalysts. We demonstrate the ammonia synthesis at mild conditions with a catalyst never employed for this purpose, i.e., molten Ga, resulting in an ammonia yield of 10% and an energy yield of 0.22 g-NH_3/kWh. We also explored conventional transition metals for this reaction, such as Pd, Ag, Au, Fe, and Cu. This allowed us to obtain unprecedented ammonia yields up to 19%, surpassing the yield for the Haber-Bosch process. However, the energy yield of 0.2 g-NH_3/kWh and energy cost of 229 MJ/mol need to be greatly improved. It is important to mention that the main purpose of this work was to obtain more fundamental insight in the underlying mechanisms. For this purpose, we developed a chemical kinetics model to elucidate the most important reaction pathways of ammonia synthesis. Furthermore, by means of operando UV−vis spectrometry, we could demonstrate experimentally the interaction of the gas phase species with the catalyst surface, which results in the enhanced processing of the gas input stream, or the plasma catalytic effect.

ASSOCIATED CONTENT

Supporting Information

The Supporting Information is available free of charge on the ACS Publications website at DOI: 10.1021/acsaem.8b00898.

More information about the experiments, emission spectroscopy, and the model (PDF)

AUTHOR INFORMATION

Corresponding Authors

*E-mail: annemie.bogaerts@uantwerpen.be.
*E-mail: maria-carreon@utulsa.edu.

ORCID

Annemie Bogaerts: 0000-0001-9875-6460
Maria L. Carreon: 0000-0002-2717-1577

Author Contributions

J.S. and W.W. contributed equally and are shared first author. The manuscript was written through contributions of all authors.

Notes

The authors declare no competing financial interest.

ACKNOWLEDGMENTS

M.L.C. acknowledges financial support from The University of Tulsa Faculty Startup Funds and The University of Tulsa Faculty Development Summer Fellowship Grant (FDSF). A.B. acknowledges financial support from the Excellence of Science program of the Fund for Scientific Research (FWO-FNRS; Grant no. G0F91618N; EOS ID 30505023). The calculations were performed using the Turing HPC infrastructure at the CalcUA core facility of the Universiteit Antwerpen (UAntwerpen), a division of the Flemish Supercomputer Center VSC, funded by the Hercules Foundation, the Flemish Government (department EWI) and the UAntwerpen.

REFERENCES

(1) Patil, B. S. *Plasma (Catalyst)—Assisted Nitrogen Fixation: Reactor Development of Nitric Oxide and Ammonia Production*; Technische Universiteit Eindhoven: Eindhoven, 2017.
(2) Appl, M. *Ullmann's Encyclopedia of Industrial Chemistry*; Wiley, 2012, 139−225.
(3) Bogaerts, A.; Neyts, E. C. Plasma Technology: An Emerging Technology for Energy Storage. *ACS Energy Lett.* **2018**, *3*, 1013−1027.
(4) Marnellos, G.; Stoukides, M. Ammonia Synthesis at Atmospheric Pressure. *Science* **1998**, *282*, 98−100.
(5) Schlögl, R. *Ammonia Synthesis*; Wiley Online Library, 2008.
(6) Smil, V. *Enriching the Earth: Fritz Haber, Carl Bosch, and the Transformation of World Food Production*; MIT Press, 2004.
(7) Tanabe, Y.; Nishibayashi, Y. Developing More Sustainable Processes for Ammonia Synthesis. *Coord. Chem. Rev.* **2013**, *257*, 2551−2564.
(8) Schrock, R. R. Reduction of Dinitrogen. *Proc. Natl. Acad. Sci. U. S. A.* **2006**, *103*, 17087−17087.
(9) Global-Ammonia-Capacity-to-Reach-Almost-250-Million-Tons-per-Year-by-2018-Says-Global data. http://energy.globaldata.com/media-center/press-releases/oil-and-gas/ (accessed May 2018).
(10) Kandemir, T.; Schuster, M. E.; Senyshyn, A.; Behrens, M.; Schlögl, R. The Haber−Bosch Process Revisited: on the Real Structure and Stability of "Ammonia Iron" under Working Conditions. *Angew. Chem., Int. Ed.* **2013**, *52*, 12723−12726.
(11) Howard, J. B.; Rees, D. C. Structural Basis of Biological Nitrogen Fixation. *Chem. Rev.* **1996**, *96*, 2965−2982.
(12) Wang, W.; Patil, B.; Heijkers, S.; Hessel, V.; Bogaerts, A. Nitrogen Fixation by Gliding Arc Plasma: Better Insight by Chemical Kinetics Modelling. *ChemSusChem* **2017**, *10*, 2145−2157.
(13) Ertl, G.; Lee, S.; Weiss, M. Adsorption of Nitrogen on Potassium Promoted Fe (111) and (100) Surfaces. *Surf. Sci.* **1982**, *114*, 527−545.
(14) Massey, H. S. W.; Massey, H. S. W. *Negative Ions*; CUP Archive, 1976.
(15) Chase, M. W.; Davies, C. A.; Downe, J. R.; Frurip, D. J.; McDonald, R. A.; Syverue, A. N *J. Phys. Chem. Ref. Data* **1985**, *14* (Suppl 1), 1−1856.
(16) Rosenstock, H. M.; D, K.; Steiner, B. W.; Herron, J. T. J. *Phys. Chem. Ref. Data* **1977**, *6*, 1253.
(17) Huheey, J.; Cottrell, T. *The Strengths of Chemical Bonds*; Butterworths, 1958.
(18) Hellman, A.; Baerends, E.; Biczysko, M.; Bligaard, T.; Christensen, C. H.; Clary, D.; Dahl, S.; Van Harrevelt, R.; Honkala, K.; Jonsson, H. *Predicting Catalysis: Understanding Ammonia Synthesis from First-Principles Calculations*; ACS Publications, 2006.
(19) Rees, D. C.; Howard, J. B.; et al. Structural basis of biological nitrogen fixation. *Philos. Trans. R. Soc., A* **2005**, *363*, 971−984.
(20) Jensen, J. O.; Vestbø, A. P.; Li, Q.; Bjerrum, N. The Energy Efficiency of Onboard Hydrogen Storage. *J. Alloys Compd.* **2007**, *446-447*, 723−728.

DOI: 10.1021/acsaem.8b00898
ACS Appl. Energy Mater. 2018, 1, 4824−4839

(21) Saika, T.; Nakamura, M.; Nohara, T.; Ishimatsu, S. Study of Hydrogen Supply System with Ammonia Fuel. *JSME Int. J., Ser. B* **2006**, *49*, 78−83.
(22) Zamfirescu, C.; Dincer, I. Ammonia as a Green Fuel and Hydrogen Source for Vehicular Applications. *Fuel Process. Technol.* **2009**, *90*, 729−737.
(23) Kroch, E. Ammonia−A Fuel for Motor Buses. *J. Inst. Pet.* **1945**, *31*, 213−223.
(24) Klerke, A.; Christensen, C. H.; Nørskov, J. K.; Vegge, T. Ammonia for Hydrogen Storage: Challenges and Opportunities. *J. Mater. Chem.* **2008**, *18*, 2304−2310.
(25) Rees, N. V.; Compton, R. G. Carbon-Free Energy: A Review of Ammonia-and Hydrazine-Based Electrochemical Fuel Cells. *Energy Environ. Sci.* **2011**, *4*, 1255−1260.
(26) Schlapbach, L.; Züttel, A. Hydrogen-Storage Materials for Mobile Applications. *Nature* **2001**, *414*, 353−358.
(27) Christensen, C. H.; Johannessen, T.; Sørensen, R. Z.; Nørskov, J. K. Towards an Ammonia-Mediated Hydrogen Economy? *Catal. Today* **2006**, *111*, 140−144.
(28) Lan, R.; Irvine, J. T.; Tao, S. Ammonia and Related Chemicals as Potential Indirect Hydrogen Storage Materials. *Int. J. Hydrogen Energy* **2012**, *37*, 1482−1494.
(29) Cortright, R. D.; Davda, R.; Dumesic, J. A. Hydrogen from Catalytic Reforming of Biomass-derived Hydrocarbons in Liquid Water. *Nature* **2002**, *418*, 964−967.
(30) Bai, M.; Zhang, Z.; Bai, X.; Bai, M.; Ning, W. Plasma Synthesis of Ammonia with a Microgap Dielectric Barrier Discharge at Ambient Pressure. *IEEE Trans. Plasma Sci.* **2003**, *31*, 1285−1291.
(31) Neyts, E. C.; Ostrikov, K.; Sunkara, M. K.; Bogaerts, A. Plasma Catalysis: Synergistic Effects at the Nanoscale. *Chem. Rev.* **2015**, *115*, 13408−13446.
(32) Whitehead, J. C. Plasma−Catalysis: the Known Knowns, the Known Unknowns and the Unknown Unknowns. *J. Phys. D: Appl. Phys.* **2016**, *49*, 243001.
(33) Nakajima, J.; Sekiguchi, H. Synthesis of Ammonia using Microwave Discharge at Atmospheric Pressure. *Thin Solid Films* **2008**, *516*, 4446−4451.
(34) Uyama, H.; Matsumoto, O. Synthesis of Ammonia in High-Frequency Discharges. *Plasma Chem. Plasma Process.* **1989**, *9*, 13−24.
(35) Van Helden, J.; Wagemans, W.; Yagci, G.; Zijlmans, R.; Schram, D.; Engeln, R.; Lombardi, G.; Stancu, G.; Röpcke, J. Detailed Study of the Plasma-Activated Catalytic Generation of Ammonia in N 2-H 2 Plasmas. *J. Appl. Phys.* **2007**, *101*, 043305.
(36) Mizushima, T.; Matsumoto, K.; Ohkita, H.; Kakuta, N. Catalytic effects of metal-loaded membrane-like alumina tubes on ammonia synthesis in atmospheric pressure plasma by dielectric barrier discharge. *Plasma Chem. Plasma Process.* **2007**, *27*, 1−11.
(37) Gomez-Ramirez, A.; Cotrino, J.; Lambert, R.; González-Elipe, A. Efficient Synthesis of Ammonia from N2 and H2 Alone in a Ferroelectric Packed-bed DBD Reactor. *Plasma Sources Sci. Technol.* **2015**, *24*, 065011.
(38) Aihara, K.; Akiyama, M.; Deguchi, T.; Tanaka, M.; Hagiwara, R.; Iwamoto, M. Remarkable Catalysis of a Wool-like Copper Electrode for NH 3 Synthesis from N 2 and H 2 in Non-Thermal Atmospheric Plasma. *Chem. Commun.* **2016**, *52*, 13560−13563.
(39) Gordiets, B.; Ferreira, C.; Pinheiro, M.; Ricard, A. Self-Consistent Kinetic Model of Low-Pressure-Flowing Discharges: II. Surface Processes and Densities of N, H, Species. *Plasma Sources Sci. Technol.* **1998**, *7*, 379.
(40) Gómez-Ramírez, A.; Montoro-Damas, A. M.; Cotrino, J.; Lambert, R. M.; González-Elipe, A. R. About the Enhancement of Chemical Yield during the Atmospheric Plasma Synthesis of Ammonia in a Ferroelectric Packed Bed Reactor. *Plasma Processes Polym.* **2017**, *14*, 1600081.
(41) Akay, G.; Zhang, K. Process Intensification in Ammonia Synthesis Using Novel Coassembled Supported Microporous Catalysts Promoted by Nonthermal Plasma. *Ind. Eng. Chem. Res.* **2017**, *56*, 457−468.
(42) Uyama, O. M. T. N. H. In *Effect of Iorn Wires on The Synthesis of Ammonia and Hydrazine in a Radio-Frequency Discharge*, International Symponisum on Plasma Chemistry, Bochum, Germany; 1991; pp 2.3−9.
(43) Matsumoto, O. Plasma Catalytic Reaction in Ammonia Synthesis in the Microwave Discharge. *J. Phys. IV* **1998**, *8*, Pr7-411.
(44) Tanaka, S.; Uyama, H.; Matsumoto, O. Synergistic Effects of Catalysts and Plasmas on the Synthesis of Ammonia and Hydrazine. *Plasma Chem. Plasma Process.* **1994**, *14*, 491−504.
(45) Uyama, H.; Nakamura, T.; Tanaka, S.; Matsumoto, O. Catalytic Effect of Iron Wires on the Syntheses of Ammonia and Hydrazine in a Radio-Frequency Discharge. *Plasma Chem. Plasma Process.* **1993**, *13*, 117−131.
(46) Chen, F. F. Radiofrequency Plasma Sources for Semiconductor Processing. *Adv. Plasma Technol.* **2007**, 99−115.
(47) Kim, H. H.; Teramoto, Y.; Ogata, A.; Takagi, H.; Nanba, T. Atmospheric-Pressure Nonthermal Plasma Synthesis of Ammonia over Ruthenium Catalysts. *Plasma Processes Polym.* **2017**, *14*, 1600157.
(48) https://www.nist.gov/pml/div685/grp01/unit_conversions (accessed March 2018).
(49) Pancheshnyi, S.; Eismann, B.; Hagelaar, G.; Pitchford, L. *Computer Code ZDPlasKin*; University of Toulouse, LAPLACE, CNRS-UPS-INP: Toulouse, France, 2008.
(50) Carrasco, E.; Jiménez-Redondo, M.; Tanarro, I.; Herrero, V. J. Neutral and Ion Chemistry in Low Pressure DC Plasmas of H 2/N 2 Mixtures: Routes for the Efficient Production of NH3 and NH 4+. *Phys. Chem. Chem. Phys.* **2011**, *13*, 19561−19572.
(51) Hong, J.; Pancheshnyi, S.; Tam, E.; Lowke, J. J.; Prawer, S.; Murphy, A. B. Kinetic Modelling of NH3 Production in N2−H2 Non-Equilibrium Atmospheric-Pressure Plasma Catalysis. *J. Phys. D: Appl. Phys.* **2017**, *50*, 154005.
(52) Kim, Y. C.; Boudart, M. Recombination of Oxygen, Nitrogen, and Hydrogen Atoms on Silica: Kinetics and Mechanism. *Langmuir* **1991**, *7*, 2999−3005.
(53) Bikerman, J. J. *Surface Chemistry: Theory and Applications*; Elsevier, 2013.
(54) Carolus, M. D.; Bernasek, S. L.; Schwartz, J. Measuring the surface roughness of sputtered coatings by microgravimetry. *Langmuir* **2005**, *21*, 4236−4239.
(55) Chantry, P. A Simple Formula for Diffusion Calculations Involving Wall Reflection and Low Density. *J. Appl. Phys.* **1987**, *62*, 1141−1148.
(56) Gordiets, B.; Ferreira, C.; Pinheiro, M.; Ricard, A. Self-Consistent Kinetic Model of Low-Pressure-Flowing Discharges: I. Volume Processes. *Plasma Sources Sci. Technol.* **1998**, *7*, 363.
(57) Stoltze, P.; Nørskov, J. An Interpretation of the High-Pressure Kinetics of Ammonia Synthesis Based on a Microscopic Model. *J. Catal.* **1988**, *110*, 1−10.
(58) Cortright, R.; Dumesic, J. Kinetics of Heterogeneous Catalytic Reactions: Analysis of Reaction Schemes. *Adv. Catal.* **2001**, *46*, 161−264.
(59) Jiménez-Redondo, M.; Carrasco, E.; Herrero, V. J.; Tanarro, I. Isotopic Exchange Processes in Cold Plasmas of H 2/D 2 Mixtures. *Phys. Chem. Chem. Phys.* **2011**, *13*, 9655−9666.
(60) Ertl, G. Surface Science and Catalysis—Studies on the Mechanism of Ammonia Synthesis: the PH Emmett Award Address. *Catal. Rev.: Sci. Eng.* **1980**, *21*, 201−223.
(61) Lieberman, M. A.; Lichtenberg, A. J. *Principles of Plasma Discharges and Materials Processing*; John Wiley & Sons, 2005.
(62) Harrison, L.; Bamford, C.; Tipper, C. The Theory of Kinetics. *Comprehensive Chemical Kinetics* **1969**, *2*, 377.
(63) Marinov, D. *Reactive Adsorption of Molecules and Radicals on Surfaces under Plasma Exposure*; Ecole Polytechnique X, 2012.
(64) Hansen, F. Y.; Henriksen, N. E.; Billing, G. D.; Guldberg, A. Catalytic Synthesis of Ammonia using Vibrationally Excited Nitrogen Molecules: Theoretical Calculation of Equilibrium and Rate Constants. *Surf. Sci.* **1992**, *264*, 225−234.

DOI: 10.1021/acsaem.8b00898
ACS Appl. Energy Mater. 2018, 1, 4824−4839

(65) Billing, G. D.; Guldberg, A.; Henriksen, N. E.; Hansen, F. Y. Dissociative Chemisorption of N2 on Rhenium: Dynamics at Low Impact Energies. *Chem. Phys.* **1990**, *147*, 1−11.
(66) Rettner, C.; Stein, H. Effect of Vibrational Energy on the Dissociative Chemisorption of N2 on Fe (111). *J. Chem. Phys.* **1987**, *87*, 770−771.
(67) Oinuma, G.; Inanaga, Y.; Tanimura, Y.; Kuzumoto, M.; Tabata, Y.; Watanabe, K. A Comparative Study of the Surface Recombination of Nitrogen Atoms on Various Materials at Atmospheric Pressure. *J. Phys. D: Appl. Phys.* **2010**, *43*, 255202.
(68) Mehta, P.; Barboun, P.; Herrera, F. A.; Kim, J.; Rumbach, P.; Go, D. B.; Hicks, J. C.; Schneider, W. F. Overcoming Ammonia Synthesis Scaling Relations with Plasma-Enabled Catalysis. *Nature Catal* **2018**, *1*, 269.
(69) Carter, R. G. RF Power Generation. *CERN Yellow Report* **2011**, 173−207.
(70) Huang, H.; Tang, L. Treatment of Organic Waste using Thermal Plasma Pyrolysis Technology. *Energy Convers. Manage.* **2007**, *48*, 1331−1337.
(71) Snoeckx, R.; Bogaerts, A. Plasma Technology−a Novel Solution for CO 2 Conversion? *Chem. Soc. Rev.* **2017**, *46*, 5805−5863.
(72) Mingdong, B.; Xiyao, B.; Zhitao, Z.; Mindi, B. Synthesis of Ammonia in a Strong Electric Field Discharge at Ambient Pressure. *Plasma Chem. Plasma Process.* **2000**, *20*, 511−520.
(73) Peng, P.; Cheng, Y.; Hatzenbeller, R.; Addy, M.; Zhou, N.; Schiappacasse, C.; Chen, D.; Zhang, Y.; Anderson, E.; Liu, Y.; et al. Ru-Based Multifunctional Mesoporous Catalyst for Low-Pressure and Non-Thermal Plasma Synthesis of Ammonia. *Int. J. Hydrogen Energy* **2017**, *42*, 19056−19066.
(74) Mizushima, T.; Matsumoto, K.; Sugoh, J.-i.; Ohkita, H.; Kakuta, N. Tubular Membrane-like Catalyst for Reactor with Dielectric-Barrier-Discharge Plasma and its Performance in Ammonia Synthesis. *Appl. Catal., A* **2004**, *265*, 53−59.
(75) Carreon, M. L.; Jaramillo-Cabanzo, D. F.; Chaudhuri, I.; Menon, M.; Sunkara, M. K. Synergistic Interactions of H2 and N2 with Molten Gallium in the Presence of Plasma. *J. Vac. Sci. Technol., A* **2018**, *36*, 021303.
(76) Modak, J. M. Haber Process for Ammonia Synthesis. *Resonance* **2002**, *7*, 69−77.
(77) Kim, H.-H.; Teramoto, Y.; Ogata, A.; Takagi, H.; Nanba, T. Plasma Catalysis for Environmental Treatment and Energy Applications. *Plasma Chem. Plasma Process.* **2016**, *36*, 45−72.
(78) Cherkasov, N.; Ibhadon, A.; Fitzpatrick, P. A Review of the Existing and Alternative Methods for Greener Nitrogen Fixation. *Chem. Eng. Process.* **2015**, *90*, 24−33.
(79) Calzada, M.; Moisan, M.; Gamero, A.; Sola, A. Experimental Investigation and Characterization of the Departure from Local Thermodynamic Equilibrium Along a Surface-wave-sustained Discharge at Atmospheric Pressure. *J. Appl. Phys.* **1996**, *80*, 46−55.
(80) Samukawa, S.; Hori, M.; Rauf, S.; Tachibana, K.; Bruggeman, P.; Kroesen, G.; Whitehead, J. C.; Murphy, A. B.; Gutsol, A. F.; Starikovskaia, S.; et al. The 2012 Plasma Roadmap. *J. Phys. D: Appl. Phys.* **2012**, *45*, 253001.
(81) Godyak, V.; Chung, C.-W. Distributed Ferromagnetic Inductively Coupled Plasma as an Alternative Plasma Processing Tool. *Jpn. J. Appl. Phys.* **2006**, *45*, 8035.
(82) Mehdizadeh, M. *Microwave/RF Applicators and Probes: For Material Heating, Sensing, and Plasma Generation*. William Andrew, 2015.
(83) Sakamoto, Y.; Maeno, S.; Tsubouchi, N.; Kasuya, T.; Wada, M. Comparison of Plasma Parameters in CCP and ICP Processes Appropriate for Carbon Nanotube Growth. *J. Plasma Fusion Res.* **2009**, *8*, 587−90.
(84) Fridman, A. *Plasma Chemistry*; Cambridge University Press, 2008.
(85) Iwamoto, M.; Akiyama, M.; Aihara, K.; Deguchi, T. Ammonia Synthesis on Wool-Like Au, Pt, Pd, Ag, or Cu Electrode Catalysts in Nonthermal Atmospheric-Pressure Plasma of N2 and H2. *ACS Catal.* **2017**, *7*, 6924−6929.
(86) Gladysz, J. A. Recoverable Catalysts. Ultimate Goals, Criteria of Evaluation, and the Green Chemistry Interface. *Pure Appl. Chem.* **2001**, *73*, 1319−1324.
(87) Astruc, D. *Nanoparticles and Catalysis*; John Wiley & Sons, 2008.
(88) Bai, M.; Zhang, Z.; Bai, M.; Bai, X.; Gao, H. Conversion of Methane to Liquid Products, Hydrogen, and Ammonia with Environmentally Friendly Condition-Based Microgap Discharge. *J. Air Waste Manage. Assoc.* **2008**, *58*, 1616−1621.
(89) Fuchs, P. Low-Pressure Plasma Cleaning of Au and PtIr Noble Metal Surfaces. *Appl. Surf. Sci.* **2009**, *256*, 1382−1390.
(90) Belkind, A.; Gershman, S. Plasma Cleaning of Surfaces. *Vacuum Coating and Technology* **2008**, 46−57.

DOI: 10.1021/acsaem.8b00898
ACS Appl. Energy Mater. 2018, 1, 4824−4839